Journal of Mechatronics, Electrical Power, and Vehicular Technology 17 (2026) 128-154

Journal of Mechatronics, Electrical Power, and Vehicular Technology

e-ISSN: 2088-6985
p-ISSN: 2087-3379

mev.brin.go.id

Development of a human wrist joint rehabilitation robot with AFC-PID control

Abbas Moloody [a, *], Mohammad Mahjoob [b], Azizan As'arry [a], Mohd Zarhamdy Mohd Zain [c]

[a] Department of Mechanical and Manufacturing Engineering, Universiti Putra Malaysia UPM, Serdang, 43400, Malaysia

[b] School of Mechanical Engineering, College of Engineering, Center for Advanced Orthopedic Studies BIDMC, HMS, Harvard University, Boston, MA 002215, United States of America

[c] Department of Applied Mechanics and Design, Universiti Teknologi Malaysia Jalan Sultan Yahya Petra, Kuala Lumpur, 54100, Malaysia

Abstract

Robotics is transforming healthcare rehabilitation by improving precision, efficiency, and accessibility. While industrial robots are widely used, service robots in medical applications remain underutilized. Wrist rehabilitation is essential for restoring mobility and strength after injury or surgery. This study presents a three degrees of freedom (DOF) robotic system designed to assist patients with wrist mobility impairments, aiming to enhance rehabilitation outcomes. This study develops a 3-DOF wrist rehabilitation robot with active force control – proportional-integral-derivative (AFC-PID) control to enhance rehabilitation outcomes. Traditional rehabilitation methods for wrist impairments are time-consuming, physically demanding, and inconsistent. Patients require structured therapy to reduce stiffness, receive corrective assistance for incomplete movements, and strengthen muscles. The limitations of conventional treatments create a need for more efficient and accessible therapeutic solutions. The robotic system operates in three phases: phase 1 (passive mode) where the robot aids wrist movement to relax muscles, phase 2 (assisted mode) where the robot provides compensatory force for incomplete movements, and phase 3 (strengthening mode) where the robot applies resistance to build muscle strength. The robot operates in passive, assistive, and resistive modes. Force-sensitive resistor (FSR) sensors measure interaction forces, and control is implemented via ATMEGA 32 microcontroller. Simulation and experimental trials with male and female participants were conducted. A microcontroller regulates the torque, force, angular acceleration, angular velocity and angular magnitude and direction using a PID control strategy, which is applied in accordance with therapeutic protocols. Experimental results demonstrate that the system effectively reduces stiffness, assists movement completion, and strengthens muscles through controlled resistance. The robot achieves maximum torque of 1.00 N·m, angular velocity 0.55 rad/s, and high repeatability (intraclass correlation coefficient (ICC) > 0.98 . Mode C shows active engagement with performance approaching reference values. Automating rehabilitation improves treatment efficiency and accessibility, offering a promising solution for patient recovery. The system provides adaptive, reliable, and gender-independent wrist rehabilitation, demonstrating clinical potential. The developed 3-DOF wrist rehabilitation robot with AFC-PID control achieves a maximum torque of 1.00 N·m, angular velocity of 0.55 rad/s, and reduces perceived joint stiffness by up to 15 %, demonstrating precise, adaptive assistance across passive, assistive, and resistive modes.

Keywords: active force control–proportional-integral-derivative (AFC-PID); force-sensitive resistor (FSR) sensor; joint stiffness assessment; muscle strengthening mode; wrist rehabilitation robot.

* Corresponding Author. a.moloody@gmail.com (A. Moloody)

https://doi.org/10.55981/j.mev.2026.1249

Received 13 October 2025; revised 10 March 2026; accepted 31 March 2026; available online 29 July 2026; published 31 July 2026

How to Cite: A. Moloody *et al.*, "Development of a human wrist joint rehabilitation robot with-AFC-PID control," *Journal of Mechatronics, Electrical Power, and Vehicular Technology*, vol. 17, no. 1, pp. 128-154, July, 2026.

I. Introduction

Many robots today are used in industrial manufacturing, replacing humans to reduce fatigue, delays, and risks. While their use in industry is rapidly increasing, their application in other fields, especially medicine, remains limited. Medical robotics holds great potential to improve healthcare, enhancing the quality and precision of services like surgery and rehabilitation. Conditions such as stroke, spinal cord injury, and traumatic brain injury often impair the brain's ability to control muscles rather than damaging the muscles themselves. Rehabilitation does not reverse these conditions but helps retrain the brain to regain control over healthy muscles. However, long-term treatment and access to rehabilitation centers remain major challenges for many stroke patients. The wrist joint is one of the most important joints in the body, playing a vital role in performing complex and precise hand movements. Disorders of the wrist joint, such as neurological damage, stroke, and various diseases, can lead to severe limitations in the movement of this joint. These issues not only impact the quality of life of patients but also make their rehabilitation process complex and time-consuming. In designing a wrist joint rehabilitation robot, key parameters such as force, torque, angle, velocity, and acceleration are crucial for performance in the normal, assistive, and augmentative modes. Forces must be calibrated to prevent damage, while torque should be higher in assistive and augmentative modes. Joint angles should replicate natural hand movements, and velocity must be controlled for smooth motion, especially in the augmentative mode. Acceleration should be monitored to avoid excessive movement. These parameters are extensively studied in the design of rehabilitation robots. Torque provides movement power, force ensures injury prevention, and angle calculations mimic human hand movements. The control system regulates torque, velocity, and acceleration, often using proportional-integral-derivative (PID), adaptive control, or machine learning algorithms. These factors are essential for optimal performance and user trust. A rehabilitation robot assists patients in restoring motor function by replicating therapist-guided exercises with precision and adaptability, enhancing recovery efficiency [1][2][3].

As importance of robotic rehabilitation in medical treatments, the use of robotic rehabilitation in medicine, particularly for treating wrist joint disorders, has emerged as an innovative and efficient method. Robots can provide precise and controlled corrective movements to patients, which can help accelerate the rehabilitation process. In addition to improving accuracy and efficiency, this technology enables repetitive and consistent physical exercises that surpass traditional manual rehabilitation techniques. Stroke is the most prevalent and debilitating neurological disorder in adults, characterized by sudden neurological deficits due to impaired cerebral blood supply. It ranks as the third leading cause of mortality worldwide, following cardiovascular diseases and cancer, accounting for 10 % to 12 % of all deaths [1]. Over 50 % of stroke survivors experience long-term disabilities, primarily affecting motor coordination and postural tone. Stroke is classified into ischemic (70 %), hemorrhagic (20 %), and unspecified (10 %) types [1][2]. Hemiplegia, or unilateral paralysis, is a common consequence, significantly impairing functional independence. Rehabilitation is essential for enhancing physical, emotional, social, and psychological well-being in stroke patients. Studies confirm its efficacy in improving functional capabilities [3]. Neurological disorders and aging often lead to paralysis, affecting essential activities such as movement, eating, and walking. In the U.S., approximately 250,000 individuals have sustained spinal cord injuries since 1990, with 11,000 new cases annually, nearly half experiencing upper limb paralysis [4]. Unlike stroke, which predominantly affects older adults, spinal cord injuries have an average onset age of 32 years, with treatment costs estimated at $9.73 billion. Rehabilitation exercises typically involve therapists mobilizing affected muscles and joints to restore function. However, these exercises are often time-consuming, costly, physically demanding, and imprecise. Robotic rehabilitation systems offer an efficient alternative, enhancing rehabilitation accuracy and effectiveness while reducing the burden on therapists. This study presents a wrist rehabilitation robot designed to assist patients with wrist joint disabilities. The robot operates in three degrees of freedom (DOF) and supports rehabilitation in an upright position. It performs in three phases: first, it moves the wrist in six directions to engage smooth muscles; second, it applies corrective force to assist movement when needed; and third, it provides resistance to strengthen muscles. Force direction and magnitude are controlled via programming and a proportional (P) controller in the final phase.

As challenges and limitations of traditional treatment methods, traditional rehabilitation methods, such as manual physiotherapy, can sometimes be time-consuming and inefficient. Moreover, these methods may not provide precise control over the joint's movements in all cases. Therefore, there is a need for automated and intelligent systems to correct joint movements and accelerate the rehabilitation process. Disability, whether congenital or acquired, remains a critical global issue, affecting an individual's ability to perform routine activities. the World Health Organization (WHO) defines disability as any physical or psychological impairment preventing an individual from fulfilling their social role. Impairment refers to dysfunction in physical or psychological systems, such as a broken arm, while incapacity arises when this impairment hinders daily activities. For instance, nerve damage in a fractured arm may prevent writing, leading to incapacity. Disability exists along a continuum of impairment and incapacity, necessitating comprehensive intervention and support systems. This study aims to develop a robotic rehabilitation model for patients with impaired wrist joint mobility, replicating therapist-guided treatments. The research involves extracting rehabilitation patterns and therapeutic phases based on patients' physical and physiological conditions, including weight, strength, and size. An optimized rehabilitation robot will be designed to autonomously execute therapy phases without therapist intervention. The robotic system will incorporate 3-DOF at the wrist joint, enabling effective motion algorithms tailored for seated patients [3][4].

As innovation and contributions in robotic design, this study focuses on the design and implementation of a robotic system for wrist joint rehabilitation, aimed at improving the joint's function in patients with various conditions. Using advanced control algorithms and precise sensors, this robot can effectively and efficiently perform corrective and rehabilitative movements, assisting patients in regaining the range of motion and functionality of their wrist joint. This research contributes to the field of rehabilitation robotics by developing an autonomous robotic system to aid in wrist joint rehabilitation. Unlike conventional therapy, which is labor-intensive and prone to inconsistencies, this system offers enhanced precision, efficiency, and adaptability to patient-specific needs. Furthermore, assistive robotic systems improve users' functional capabilities, facilitating daily tasks. The integration of human-robot interaction enhances rehabilitation outcomes, leveraging combined capabilities that neither humans nor robots can achieve independently. These systems differ in mechanical structure, human-robot interaction, and control methodologies [5], allowing for a more personalized and adaptive rehabilitation process.

As advancements in rehabilitation robotics, rehabilitation robots aid motor recovery through adaptive training and human-robot interaction, but challenges in control, sensors, and feedback remain. Over the past two decades, rehabilitation robotics have advanced significantly, with some systems progressing to industrial production and others still in development. Despite some robots not passing all tests, many have shown promising results in clinical trials, spurring interest in enhancing motor function and motor learning. Rehabilitation robots aim to assist in compensating for motor impairments, provide targeted training, and support rehabilitation for both upper and lower limbs, facilitating adaptive training and extended therapy sessions. The rise in disabilities post-world war I and the polio epidemic led to innovations in improving the quality of life for affected individuals. Dr. Howard Rusk, a key pioneer, established the first rehabilitation center at Bellevue Hospital, marking the start of medical rehabilitation. Ancient civilizations also used therapeutic methods like heat therapy and massage, which were later recognized for their therapeutic benefits. Various tools assess rehabilitation outcomes, such as the Jebsen-Taylor hand function test (JTHFT) for hand impairments, the medical instrumentation evaluation (MIE) system for grip strength, and goniometers and dynamometers for joint range and muscle strength. Human-robot interaction involves mutual interaction, where both the robot and the patient influence each other, managed by high-level control systems [6][7]. This interaction is categorized into perceptual and physical types [8], as shown in Figure 1.

As historical background and early developments, wearable robots for industrial and medical applications were first studied in the 1960s and 1970s [8], initially designed to enhance human strength [9]. In recent years, the focus has shifted towards rehabilitation and assisted movement for daily activities [10]. Many of these robots have high DOF, making them inherently heavy and complex, often requiring a fixed workstation for operation. Consequently, only a limited number of assistive robots have been designed for use outside laboratory settings to aid patients in daily tasks [11], as depicted in Figure 2.

As current applications and challenges in rehabilitation robotics, rehabilitation robots like Armeo and Handryha provide 3-DOF and are used in treating conditions such as cerebral palsy. These robots have shown positive effects in improving joint range, flexibility, muscle strength, and reducing spasms, aiding patient recovery [12][13][14], as seen in Figure 3 and Figure 4. Most devices target neurological disorders and focus on upper and lower limb rehabilitation, with few dedicated to wrist rehabilitation. Challenges such as cost, accessibility, maintenance, and safety persist in existing systems [15]. Thus, there is a need for accessible and user-friendly rehabilitation devices that address muscular weaknesses and restore strength across diverse patient populations.

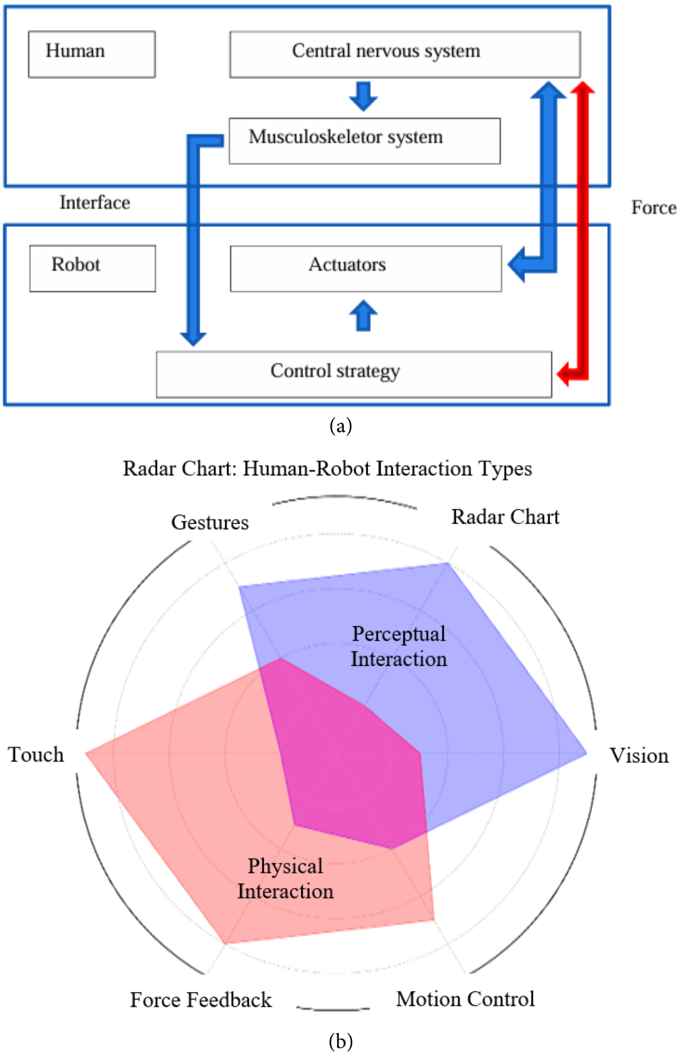

Figure 1. Difference between perceptual and physical interaction between humans and robots [7], (a) perceptual and physical of human-robot interaction and (b) radar chart of human-robot interaction types.

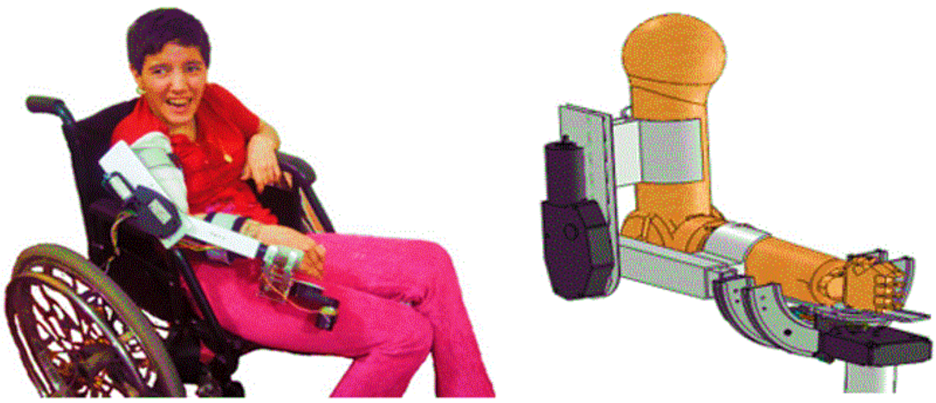

Figure 2. Wearable robots for industrial applications [11].

As system design and classification, the rehabilitation robot complies with Japan Robot Association (JIRA) and Robotics Industries Association (RIA) standards and is classified as type C and type D by the French Union of Industrial Robotics. It comprises four articulated mechanical arms, a base structure, ten sensors, a controller, a power conversion unit, and three electric stepper motor actuators. The robot serves both personal and scientific applications and falls under second- to fourth-generation control strategies. Its joint actuation system employs electric stepper motors with motion geometry based on a cylindrical coordinate system. The motion control mechanism is a non-servo type, facilitating rehabilitation for both hands in alignment with wrist joint anatomy (Figure 5 and Table 1) [16][17][18].

Figure 3. Handryha robot for the upper limb [12][13].

Figure 4. Armio robot for the upper limb [14].

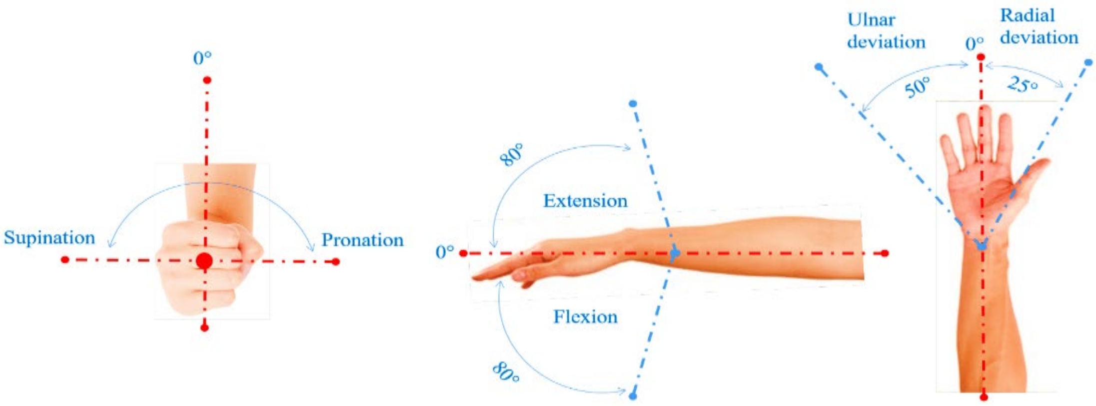

Figure 5. DOF in the human wrist [16].

Table 1.
Wrist rehabilitation robot exercises states [21][22].

Exercises States	Ulnar Deviation (°)	Radial Deviation (°)	Extension (°)	Flexion (°)	Pronation (°)	Supination (°)
1	45	15	85 to 90	85 to 90	90	90
2	50	25	80	80	90	90
3	20	20	70	70	35	35
4	25 to 30	20	50 to 70	60 to 90	80	80

II. Materials and Methods

This study develops a novel human wrist rehabilitation robot (H.W.R.R) integrating a PID controller, sensors, and actuators to facilitate structured exercises across three rehabilitation phases. The system ensures precise motion control, safety, and adaptability. Data from sensors continuously monitor accuracy, speed, and applied forces to assess rehabilitation progress.

Comparative analysis ensures the effectiveness of the system, while iterative testing, sensor calibration, and patient trials refine performance. The proposed methodology ensures an adaptive, safe, and effective rehabilitation process through precise control and real-time monitoring.

During rehabilitation sessions, patients grip the handle and perform prescribed movements to ensure systematic recovery. Experimental evaluations confirm the system's effectiveness in improving wrist mobility and strength, considering inertia, friction, and gravity (Figure 6, Figure 7 and Table 2, Table 3).

As DOF and motion control, the system operates with 3-DOF: pronation-supination (PS) mode, abduction-adduction (AA) mode, and flexion-extension (FE) mode. AA and FE modes employ distinct mechanisms, while PS mode requires coordinated actuator operation. Quantitative analysis shows PS mode has a magnitude approximately one order higher than AA and FE modes [27][28].

Three stepper motors, each dedicated to a DOF, ensure precise rotational movement. Sensors provide direct control forces to each axis, enabling rehabilitation in three modes: muscle relaxation, muscle assistance, and muscle strengthening. These modes facilitate movement in six directions, two

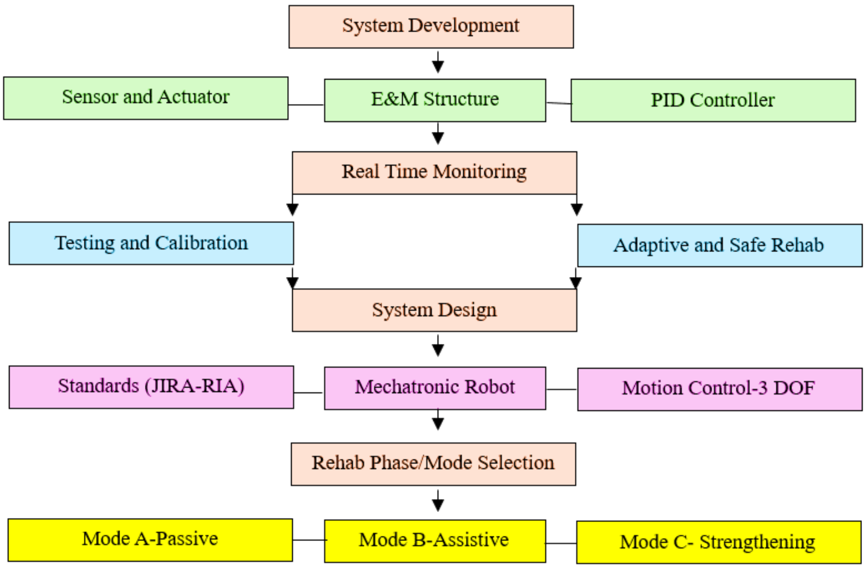

Figure 6. Methodology flowchart of wrist rehabilitation robot.

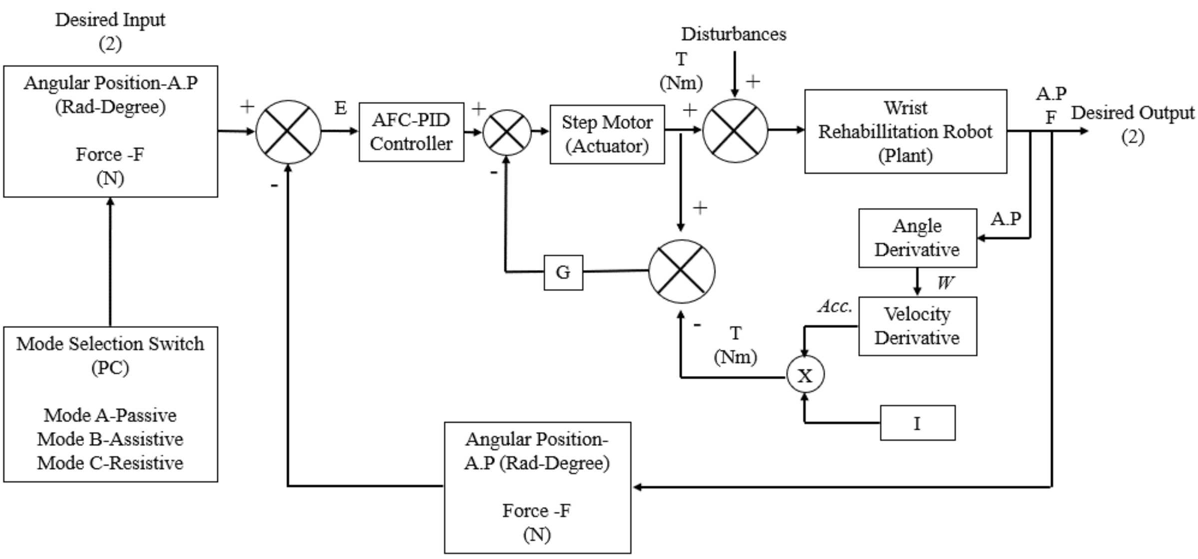

Figure 7. Control system block diagram of wrist rehabilitation robot.

horizontals (left/right), two verticals (up/down), and two rotational (clockwise (CW)/counterclockwise (CCW)), yielding 18 movement directions.

As rehabilitation exercises and phases, the robot supports structured rehabilitation exercises, including flexion, extension, abduction, adduction, supination, and pronation, following anatomical motion ranges (e.g., wrist FE ~170°, radial deviation ~15°, ulnar deviation ~40°). It assists in three rehabilitation phases (Table 2, Table 3 and Figure 6, Figure 7).

1) Phase 1: Passive rehabilitation mode (mode A)

The patient holds the handle without exerting force. The robot autonomously moves the wrist in six directions based on a predefined sequence and duration, promoting muscle relaxation. The patient can select the movement sequence and repetitions.

2) Phase 2: Assisted rehabilitation mode (mode B)

The patient actively performs exercises. If unable to achieve full motion (e.g., from the initial 0° position), the robot detects delays based on predefined time patterns (healthy individuals complete full motion in ~2 s) and compensates with assistive force.

3) Phase 3: Muscle strengthening mode (mode C)

This mode introduces resistive torque opposing motion, requiring the patient to overcome resistance to complete movements. It enhances muscle strength and assumes an average physical condition.

Table 4 summarize recent advancements in wrist rehabilitation robots (2017–2024), covering key technical specifications and research findings. The references provide detailed insights into their

Table 2.
Wrist rehabilitation robot exercises states in this research methodology [18].

Rehabilitation Phase	Mode	Ulnar Deviation (°)	Radial deviation (°)	Extension (°)	Flexion (°)	Pronation (°)	Supination (°)
Phase 1	Mode A (passive)	30 to 40 (35)	15 to 20 (17.5)	70	80	80 to 90 (85)	80 to 90 (85)
Phase 2	Mode B (assisted)	30 to 40 (35)	15 to 20 (17.5)	70	80	80 to 90 (85)	80 to 90 (85)
Phase 3	Mode C (muscle strengthening)	30 to 40 (35)	15 to 20 (17.5)	70	80	80 to 90 (85)	80 to 90 (85)

Table 3.
Technical specifications of wrist rehabilitation robots in this research [19].

Rehabilitation Phase	Mode	Torque (N·m)	Force (N)	Angular Acceleration (rad/s^2)	Angular Velocity (rad/s)	DOF
Phase 1	Mode A (passive)	0.3 to 0.9	3 to 10	1.4	0.5	3
Phase 2	Mode B (assisted)	0.4 to 1.2	5 to 12	1.6	0.55	3
Phase 3	Mode C (muscle strengthening)	0.5 to 1.5	7 to 15	1.8	0.6	3

Table 4.
Technical specifications of wrist rehabilitation robots (2017–2024).

Year	Authors	Torque (N·m)	Force (N)	Angular Acceleration (rad/s^2)	Angular Velocity (rad/s)	DOF	Key Features
2017	Lee *et al.*	0.5 to 2	5 to 30	1.5	0.5	3	AFC, portability [23]
2018	Chen *et al.*	0.2 to 1	1 to 15	1.2	0.4	6	Compact design, low-cost [24]
2019	Nguyen *et al.*	0.3 to 1.5	2 to 20	1.0	0.3	4	Virtual reality integration, force feedback [25]
2020	Zhang *et al.*	0.2 to 1	3 to 15	1.8	0.6	3	Lightweight, adjustable settings [26]
2021	Kim *et al.*	0.5 to 2.5	4 to 25	1.6	0.4	5	Advanced control algorithms, real-time feedback [27]
2022	Sharma *et al.*	0.3 to 1	2 to 12	1.3	0.4	3	Chronic pain relief, modular design [28]
2023	Wang *et al.*	0.4 to 1.5	3 to 20	1.4	0.5	4	Ergonomic, rehabilitation for elderly patients [29]
2024	Jiang *et al.*	0.5 to 3	5 to 35	2.0	0.6	6	Hybrid design, long-term monitoring [30]

effectiveness and innovations in therapy. The control block diagram represents a robotic wrist rehabilitation system designed to operate in three modes: passive, assistive, and resistive. The system takes angular position and force as desired inputs, selected through a mode switch on a PC interface. The actual angular position and force are compared with the desired values to generate an error signal, which is processed by an AFC-PID controller to produce torque commands for a stepper motor actuator.

This torque, combined with external disturbances, drives the wrist rehabilitation robot. Real-time feedback from angle and force sensors, along with derived velocity and acceleration signals, enables dynamic compensation using the active force control (AFC) technique. The outputs, angular position and force are continuously monitored to ensure accurate and safe rehabilitation movements.

A. Modelling

The modelling of a wrist joint rehabilitation robot combines kinematic and dynamic analyzes to ensure accurate movement and effective force control. Kinematic modelling addresses joint DOF and frame transformations, while dynamic modelling incorporates inertia, gravity, and friction. These models enable precise control torques and alignment with natural wrist biomechanics [31][32][33]. Force-sensitive resistors (FSRs) are placed at the robot handle to capture patient-applied forces, calibrated using a standard weight system. Torque is estimated via stepper motor current measurements and validated against known loads. The control loop, combining AFC and PID, is validated through step responses and trajectory tracking (Figure 7 and Figure 8). All variables, including $\boldsymbol{q}$ (joint positions), $\boldsymbol{\tau}$ (torques), $\mathbf{F}_{\mathrm{int}}$ (interaction forces), and $\mathbf{K}_{\mathrm{p}}$ (gain matrix), are defined in equation (12) to equation (17).

As mathematical modelling, the measurement of active stiffness in the wrist joint using the rapid release method requires precise experimental conditions that enable the subject to exert their maximum voluntary torque, which is subsequently recorded by the measurement device. This approach accounts for individual physiological and anatomical variations, as each subject exhibits unique biomechanical characteristics. Given the muscular structure of the wrist joint, individuals generate varying maximum torques based on their physiological capabilities. Following the determination of the maximum voluntary torque, the experimental setup is configured to facilitate the rapid release test. During this phase, the subject is instructed to exert maximum voluntary contraction force while the examiner introduces an unanticipated release condition without prior warning. This ensures a natural response, preventing anticipatory reflexive reactions. The hand undergoes two distinct states before and after release: initially in a stationary condition and then transitioning into dynamic motion post-release. Just before the rapid release, a balance exists between static and dynamic torque conditions. The static torque is expressed as equation (1):

$$M = F \cdot L \tag{1}$$

where F represents the voluntary contraction force and L denotes the moment arm length of the applied force. Upon release of the wrist joint, key mechanical parameters such as angular displacement and angular acceleration are measured. As wrist flexion and extension primarily involve rotational motion within a horizontal plane, the governing equations for rotation about a fixed axis apply, as given in equation (2) to equation (4) [34]:

$$F_n = m\bar{r}\omega^2 \tag{2}$$

$$F_t = m\bar{r}\alpha \tag{3}$$

$$M_O = I_O \cdot \alpha \tag{4}$$

where M_O is the torque about the center of rotation, I_O represents the moment of inertia of the system, and α denotes angular acceleration. The moment of inertia equation for a rigid body in planar motion includes an integral that accounts for mass distribution relative to the rotational axis. At the onset of movement in the rapid release phase, angular acceleration reaches its maximum value. Once this value is obtained, the system's moment of inertia can be determined. In rapid release rotational motion, stiffness is defined as the ratio of torque variation to angular position change. This relationship is expressed through equation (5) and equation (6), with the resulting stiffness formulation given in equation (7):

$$S = \frac{\Delta M}{\Delta \theta} \tag{5}$$

$$\Delta M = I \cdot \Delta \alpha \tag{6}$$

$$S = I\chi \frac{\Delta \alpha}{\Delta \theta} \tag{7}$$

This model provides a foundation for assessing wrist joint stiffness by linking mechanical parameters to physiological responses during rapid release testing. Here, the parameters definition of equation (1) to equation (7) is shown in Table 5.

As kinematic modelling of a wrist joint rehabilitation robot, calculation of wrist joint stiffness, wrist joint stiffness is determined by analyzing angular acceleration and position variations. Key parameters include maximum voluntary torque, angular position, angular acceleration, inertia, torque, and moment arm length. The student's t-test for maximum voluntary torque showed a standard deviation (SD) of 0.40523 and a p -value of 0.000, confirming statistical significance.

The coefficient of variation (CV) was 2 %, with similar trends for angular position and acceleration at 25 %, 50 %, and 75 % torque levels. Intraclass correlation coefficients (ICCs) were 0.989 for angular acceleration and 0.986 for torque, demonstrating high measurement reliability. Intra-group comparisons were analyzed using bar charts, variance analysis, and statistical metrics [35][36]. Table 6 presents the t-test results, including SD, p -value, CV, correlation

Table 5.
Parameters and definitions in equation (1) to equation (7) for wrist joint stiffness model.

Symbol	Description	Unit	Reference
M	Wrist joint torque	N·m	Classical mechanics
F	Voluntary muscle force	N	Biomechanics
L	Moment arm	m	Joint torque theory
m	Effective mass	kg	Rigid-body dynamics
r	Radius from rotation axis	m	Rotational motion
ω	Angular velocity	rad/s	Dynamics
α	Angular acceleration	rad/s²	Dynamics
$I(I_O)$	Moment of inertia	kg·m²	Rigid-body mechanics
ΔM	Torque change	N·m	Derived
$\Delta\theta$	Angular displacement change	rad	Kinematics
$\Delta\alpha$	Angular acceleration change	rad/s²	Derived
S	Wrist joint stiffness	N·m/rad	Classical mechanics

Table 6.
Results of the student's t-test for device repeatability [35].

SE	ICC	CV	*p*-value	SD	Parameter
0.000302	0.0616	0.1299	0.000	0.00144	Angle (rad)
0.000926	0.956	0.2022	0.000	0.00444	Angle (rad)
0.001343	0.972	0.1525	0.000	0.00644	Angle (rad)
0.333281	0.990	0.1300	0.000	1.598	Acceleration (m/s^2)
0.408625	0.989	0.1435	0.000	1.959	Acceleration (m/s^2)
0.39250	0.984	0.1666	0.000	1.882	Acceleration (m/s^2)
0.08450	0.996	0.0201	0.000	0.40523	Torque (N·m)

coefficients, and mean standard error (SE) for wrist joint measurements [35][36]. Since the rehabilitation robot operates entirely in joint space, computing the Jacobian matrix $\mathbf{J}(\boldsymbol{q})$ and its transpose $\mathbf{J}^{\mathrm{T}}(\boldsymbol{q})$ is essential for mapping forces and torques from operational space to joint responses. Using the robot's schematic, the Denavit-Hartenberg (DH) parameters define reference frames and facilitate forward kinematics computation. These parameters are listed in Table 7 and illustrated in Figure 8. To map the applied force from the sensor's frame (S) to the global reference system (O), the transformation is used as shown in the schematic [37][38]. $\mathbf{P}_{OS}$ is a 3×1 vector defining the position of frame S relative to frame O, and $\mathbf{R}_{OS}$ is the rotation matrix describing the orientation of frame S with respect to frame O, computed as in equation (8) and equation (9).

$$\mathbf{R}_{OS} = \mathbf{R}_{O1}(t_1)\mathbf{R}_{12}(t_2)\mathbf{R}_{2S}(t_3) \tag{8}$$

The transformation matrix maps one frame relative to another. The rotation matrices define the rotations of frame 1 with respect to frame O and frame S with respect to frame 2, and they are computed accordingly. The relationships are given by equation (10) and equation (11):

$$\mathbf{Ad}_{GOS} = \begin{bmatrix} \mathbf{R}_{OS} & \mathbf{P}_{OS} \cdot \mathbf{R}_{OS} \\ 0 & \mathbf{R}_{OS} \end{bmatrix} \tag{10}$$

$$\mathbf{F}_{\mathrm{int}} = \mathbf{Ad}_{GOS}^{\mathrm{T}} \mathbf{F}_{\mathrm{int}}^{S} \tag{11}$$

As dynamic modelling of a human wrist joint rehabilitation robot, in this study, a control algorithm for force control is developed and implemented, considering the dynamics of the rehabilitation robot, including gravity, inertia, and friction. The goal is to minimize the endpoint interaction force based on the zero-reference point. The dynamic equation of the robot is given by equation (12):

$$ {}^{i-1}_{i}\mathrm{T} = \begin{bmatrix} \cos\theta_i & -\sin\theta_i & 0 & \alpha_{i-1} \\ \sin\theta_i \cos\alpha_{i-1} & \cos\theta_i \cos\alpha_{i-1} & -\sin\alpha_{i-1} & -\sin\alpha_{i-1}\, d_i \\ \sin\theta_i \sin\alpha_{i-1} & \cos\theta_i \sin\alpha_{i-1} & \cos\alpha_{i-1} & \cos\alpha_{i-1}\, d_i \\ 0 & 0 & 0 & 1 \end{bmatrix} \tag{9}$$

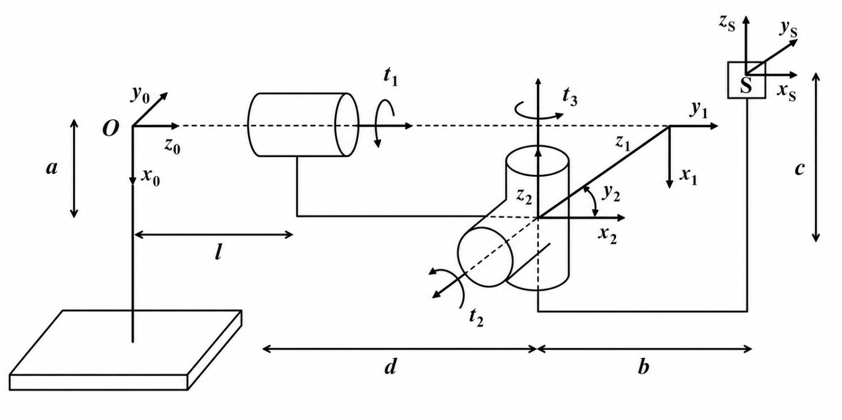

Figure 8. Schematic representation of the kinematics of the wrist joint rehabilitation robot.

Table 7.
DH parameters for the schematic kinematics of the wrist joint rehabilitation robot.

Joint	a_i (cm)	d_i (cm)	α_i (°)	θ_i (°)
1	a	d	-90	t_1
2	0	0	90	t_2
3	b	c	0	t_3

$$\mathbf{B}(\boldsymbol{q})\ddot{\boldsymbol{q}} + \boldsymbol{b}\dot{\boldsymbol{q}} + \boldsymbol{g}(\boldsymbol{q}) = \boldsymbol{\tau} - \mathbf{J}^{\mathrm{T}}(\boldsymbol{q})\mathbf{F}_{\mathrm{int}} \tag{12}$$

Here, $\mathbf{F}_{\mathrm{int}}$ is a 6×1 vector of generalized forces applied by the user, $\boldsymbol{b}$ is a 3×3 diagonal matrix of friction coefficients, $\mathbf{B}(\boldsymbol{q})$ is the inertia matrix, $\mathbf{J}^{\mathrm{T}}(\boldsymbol{q})$ is the transposed Jacobian matrix, $\boldsymbol{g}(\boldsymbol{q})$ is the gravitational term, and τ represents the control torques. The equation is divided into three scalar equations corresponding to the PS, AA, and FE joint modes. The joint coordinate vector is defined as in equation (13):

$$\boldsymbol{q} = [q_{\mathrm{PS}} \quad q_{\mathrm{AA}} \quad q_{\mathrm{FE}}]^{\mathrm{T}} \tag{13}$$

The implemented control law is expressed in equation (14) where ^ denotes an estimate, $\mathbf{F}_{\mathrm{int}}$ is the measured interaction force and $\mathbf{K}_{\mathrm{p}}$ is the positive definite gain matrix. The force error is defined in equation (15):

$$\tau = \hat{b}\dot{q} + \hat{g}(q) + \mathrm{J}^{\mathrm{T}}(q)\mathrm{F}_{\mathrm{int}} + \widehat{\mathrm{B}}(q)\mathrm{K}_{\mathrm{p}}\mathrm{J}^{\mathrm{T}}(q)(\mathrm{F}_{\mathrm{d}} - \mathrm{F}_{\mathrm{int}}) \tag{14}$$

$$\mathbf{e}_f = \mathbf{J}^{\mathrm{T}}(\boldsymbol{q})(\mathbf{F}_{\mathrm{d}} - \mathbf{F}_{\mathrm{int}}) \tag{15}$$

Substituting equation (14) into equation (12) leads to the dynamic error of the robots given by equation (16):

$$\mathbf{e}_f = \mathbf{K}_{\mathrm{p}}^{-1}\ddot{\boldsymbol{q}} \tag{16}$$

with $\mathbf{M} = \mathbf{K}_{\mathrm{p}}^{-1}$, equation (16) becomes equation (17):

$$\mathbf{e}_f = \mathbf{M}\ddot{\boldsymbol{q}} \tag{17}$$

If $\mathbf{F}_{\mathrm{d}} = 0$, the system behaves like a free body with mass $\mathbf{M}$ and increasing the P gain reduces perceived inertia, improving control performance. The force is applied only to the PS joint mode with the other two modes exhibiting reversible behavior.

Their mechanical impedance is one order smaller than the PS mode. Therefore, the control torques for the 3-DOF are as equation (18):

$$\begin{cases} \tau_{\mathrm{PS}} = \tau[1 \quad 0 \quad 0]^{\mathrm{T}} \\ \tau_{\mathrm{AA}} = 0 \\ \tau_{\mathrm{FE}} = 0 \end{cases} \tag{18}$$

For the PS mode, the control torque is given by equation (19). Finally, the control torque for the PS mode can be simplified as equation (20):

$$\tau_{\mathrm{PS}} = b_{\mathrm{PS}}\dot{q}_{\mathrm{PS}} + \tau_{\mathrm{PS}}^{g} + [\mathrm{J}^{\mathrm{T}}(q)\mathrm{F}_{\mathrm{int}} + \widehat{\mathrm{B}}(q)\mathrm{K}_{\mathrm{p}}\mathrm{J}^{\mathrm{T}}(q)(\mathrm{F}_{\mathrm{d}} - \mathrm{F}_{\mathrm{int}})][1 \quad 0 \quad 0]^{\mathrm{T}} \tag{19}$$

$$\tau_{\mathrm{PS}} = \boldsymbol{b}_{\mathrm{PS}}\dot{\boldsymbol{q}}_{\mathrm{PS}} + \tau_{\mathrm{PS}}^{g} + \tau_{\mathrm{PS}}^{\mathrm{int}} + \tau_{\mathrm{PS}}^{fb} \tag{20}$$

To implement this control scheme, the kinematic operators and dynamic properties of the rehabilitation robot must be computed, as shown in Table 6 and Table 7. Here, the parameters definition of equation (8) to equation (20) is shown in Table 8.

B. Simulation and control

In phase 1, referred to as the passive rehabilitation mode (mode A), the patient holds the robot's handle without applying any force, thereby allowing autonomous wrist movement in six directions to facilitate muscle relaxation. During this phase, the patient selects movement sequences and determines the number of repetitions. In phase 2, the assisted rehabilitation mode (mode B), the patient is required to independently execute exercises from phase 1. If the patient is unable to achieve the full range of motion, the robot detects any delays and provides compensatory force. This mode is designed to support muscle function and to assess the range of motion. Phase 3, known as the muscle strengthening mode or resistive mode (mode C), introduces resistive force opposing the motion. The patient must overcome these torques in order to complete the movements, thereby

Table 8.
Parameters and definitions in equation (8) to equation (20) for wrist joint stiffness model.

Symbol	Description	Unit	Reference
$\boldsymbol{q}$	Joint position vector [PS, AA, FE]	rad	Robot kinematics
$\dot{\boldsymbol{q}}, \ddot{\boldsymbol{q}}$	Joint velocity and acceleration	rad/s, rad/s²	Classical dynamics
τ	Control torque	N·m	Robot dynamics
$\mathbf{B}(\boldsymbol{q})$	Inertia matrix	kg·m²	Rigid-body dynamics
$\boldsymbol{b}$	Friction coefficient matrix	N·m·s/rad	Robot joint modeling
$\boldsymbol{g}(\boldsymbol{q})$	Gravity torque vector	N·m	Robot dynamics
$\mathbf{J}(\boldsymbol{q})$	Jacobian matrix	–	Manipulator kinematics
$\mathbf{F}_{\mathrm{int}}$	Human–robot interaction force	N	Force control theory
$\mathbf{F}_{\mathrm{d}}$	Desired interaction force	N	Force control
$\mathbf{K}_{\mathrm{p}}$	Proportional gain matrix	–	Impedance/AFC control
$\mathbf{M}$	Apparent inertia ($\mathbf{K}_{\mathrm{p}}^{-1}$)	kg·m²	Admittance control theory
$\mathbf{R}_{OS}$	Rotation matrix (sensor → global)	–	Coordinate transformation
$\mathbf{P}_{OS}$	Joint position vector [PS, AA, FE]	M	Coordinate transformation
$\mathbf{Ad}_{GOS}$	Joint velocity and acceleration	–	Screw theory/robotics

strengthening muscle strength. A variable resistor (potentiometer) simulates a FSR sensor. Variations in resistance affect voltage, which in turn influences pulse generation. Increased force results in a higher number of pulses and greater signal amplitude. When the handle comes into contact with the sensors, the voltage drops, halting pulse generation. Additionally, greater exertion leads to an increase in pulse width. The system uses an AFC-PID controller to operate a wrist rehabilitation robot by comparing desired and actual position and force. Sensor feedback enables precise control and disturbance rejection across passive, assistive, and resistive modes. In mode C, a microcontroller-based P controller generates resistive force proportional to pressure from the patient's hand, enhancing adaptive control (Figure 7). FSR sensor data is read via analog-to-digital converter (ADC), and when force exceeds a threshold, opposing pulses are triggered. With SP = 450, error is integrated to control the stepper motor, which locks after a 10 ms release to reflect user force. The system monitors safety via the serial port and reverses the motor if obstacles are detected. LabVIEW commands adjust settings dynamically. In mode A and mode B, 1 kHz pulses with low (L) pin settings control the motor. FSR sensors respond above 2 V. In mode C, 450 = 2.19 V is used to generate counter-pulses. Motor torque and mechanical adjustments ensure effective resistive force. FSR data analysis supports muscle recovery through adaptive resistance, Figure 9 and Figure 10, shows the hardware representation of infrared (IR) optical sensor and FSR. Unlike conventional PID controllers or standard AFC implementations, the proposed AFC-PID integrates real-time inertia estimation with adaptive torque compensation, allowing the robot to dynamically adjust resistive and assistive forces based on patient interaction, enhancing safety and motion fidelity.

The AFC module estimates the system inertia using $\mathbf{M} = \mathbf{K}_p^{-1}$ and compensates for external disturbances in real time, thereby augmenting the conventional PID controller and improving robustness and tracking performance. The overall control structure consists of a desired trajectory or reference input processed by the PID controller, followed by an AFC module responsible for inertia estimation and disturbance compensation, which generates the torque command applied to the actuator and ultimately drives the robot or plant.

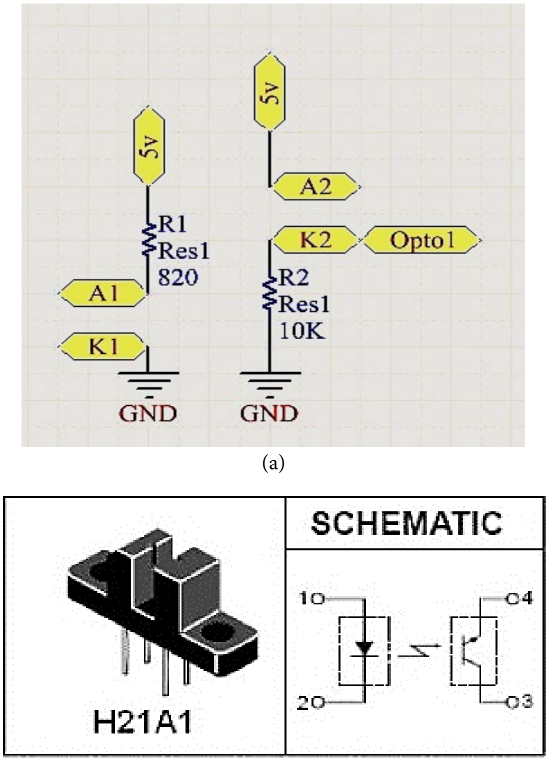

Figure 9. (a) hardware representation of the IR optical sensor; (b) electronic schematic of the human wrist joint rehabilitation robot.

C. Experimental setup

The experimental setup tested the robot's functionality, stability, and effectiveness in simulating wrist movements for rehabilitation. Using the ATMEGA 32 microcontroller and BASCOM-AVR, the robot's movements were controlled and validated for accuracy and reliability. Data on motion accuracy and user feedback were collected and analyzed, confirming the robot's ability to replicate wrist movements with minimal deviation. The results demonstrate the robot's potential to enhance rehabilitation by improving motion range and control precision. The programming of the rehabilitation robot is implemented using LabVIEW, a leading system control and data acquisition software. This program consists of a control panel and a block diagram, and it utilizes G-language for intuitive development. Functional blocks enable seamless manipulation of variables, as detailed in subsequent sections, including Figure 11, Figure 12, and Figure 13 consist of schematic and the experimental LabVIEW of the research. The rehabilitation robot's programming was done using

(a) (b)

Figure 10. (a) hardware layout of the force or pressure sensor; (b) electronic schematic of the rehabilitation robot for the human wrist joint.

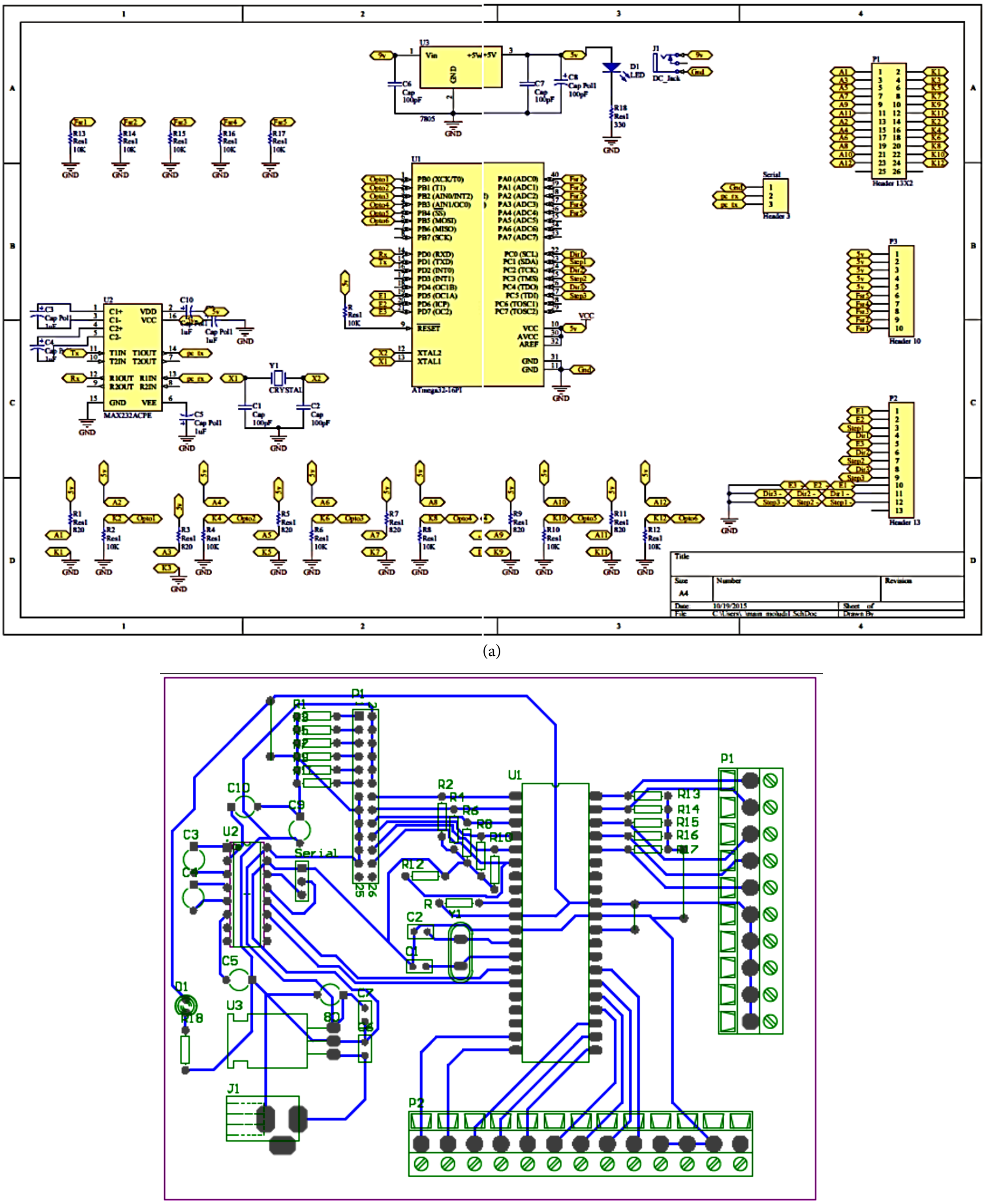

(a)

(b)

Figure 11. (a) Electronic schematic and (b) printed circuit board (PCB) layout of the human wrist joint rehabilitation robot.

BASCOM, a powerful software for AVR microcontrollers. It facilitates efficient development of control algorithms, ensuring precise robot functionality and seamless integration with embedded systems.

In addition to the t-test, repeated measures ANOVA confirmed significant differences ($p < 0.05$) in torque and acceleration across mode A, mode B, and mode C, supporting the effectiveness of the robot in progressive rehabilitation.

In mechanical design structure and considerations for the H.W.R.R, the wrist rehabilitation robot integrates mechanical, electrical, and electronic systems for precise, durable, and cost-effective performance. Its design ensures stability and simulates natural wrist movements using a vibration-reducing frame and

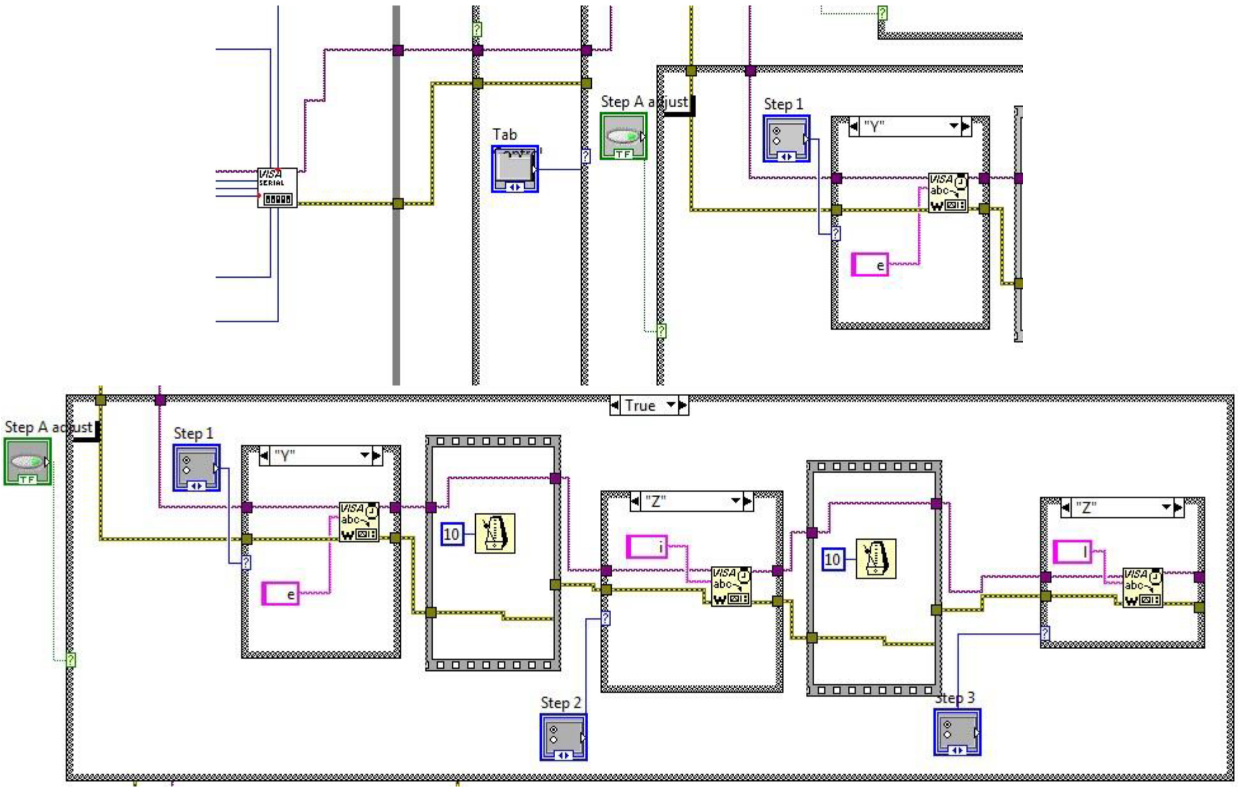

Figure 12. LabVIEW interface of the experimental setup for the human wrist joint rehabilitation robot.

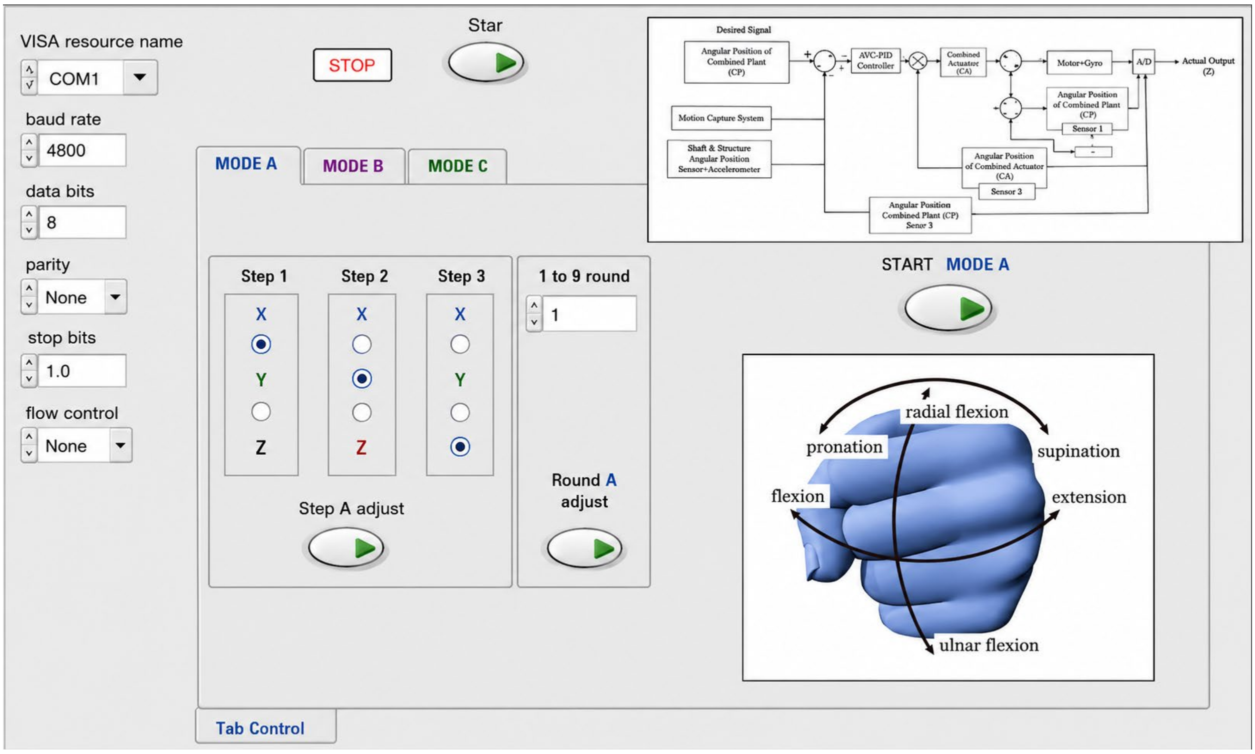

Figure 13. Control panel section of mode phases of wrist rehabilitation robot.

counterweight. The horizontal arm (axis A) enables side-to-side motion, while the vertical arm (axis B) allows flexion and extension. Both are mechanically linked for coordinated movement. The handle operates in three modes, neutral, left, and right rotation. The rotational arm (axis C) adds multi-directional movement within a semi-spherical range, enhancing wrist motion simulation. Together, axes A and B allow four-directional motion (left, right, up, down), while the addition of axis C increases the DOF to six, enabling versatile rehabilitation exercises (Figure 14, Figure 15, and Figure 16).

In electrical design structure, medical robotics and bioelectric systems, electronic components form a crucial interface between the control unit and mechanical structures. Functioning akin to the human nervous system, they transmit commands from the central controller to actuators and mechanical structures (Table 9). In control system, that often referred to as the "brain" of the robot, is essential for its proper functionality. Any malfunction or programming error can result in operational failure. In this study, an AVR microcontroller is utilized for control due to its cost-effectiveness and ease of programming.

The internal structure and command transmission process of the microcontroller are analyzed, with programming conducted using the BASCOM-AVR compiler (Table 10). Robotic control methods include human-controlled operation, computer-based control and microcontroller-based control. This research adopts microcontroller-based control as the primary method. These components work synergistically to ensure seamless integration between hardware and software, facilitating precise motion control for effective rehabilitation therapy.

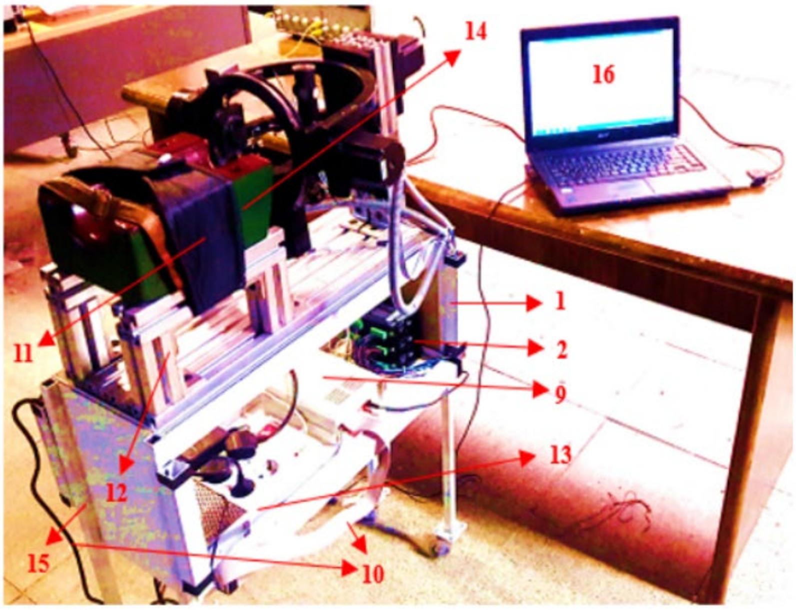

1. Dock
2. Drivers
3. Sensors
4. Vertical arm
5. Horizontal arm
6. Rotational arm
7. Stepper motor
8. Counter weight
9. Electronic board
10. Connecting cables
11. Forearm securing belt
12. Adjustable base/frame
13. Power supply and adapter
14. Adjustable forearm placement area
15. Robot device stand (four-legged base)

Figure 14. Real experimental view of rehabilitation robot device.

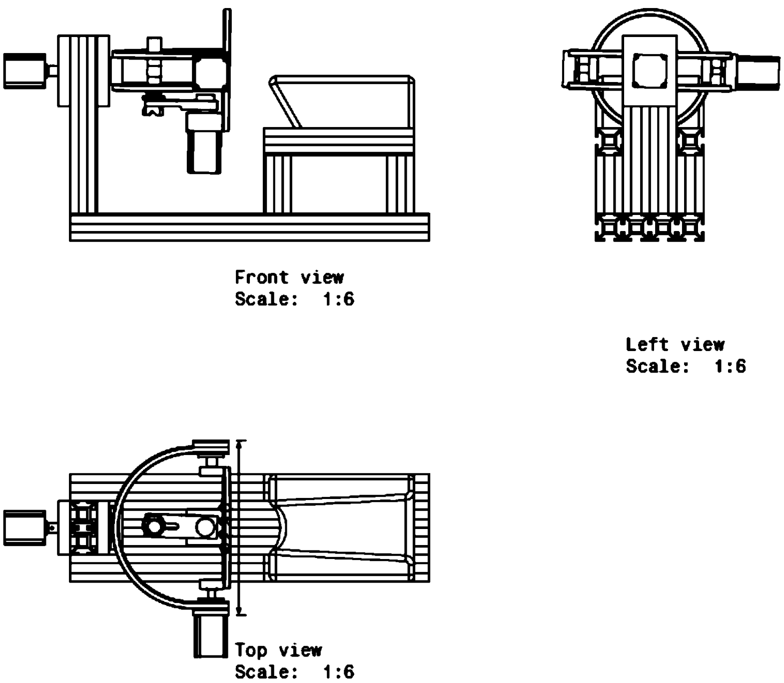

Figure 15. Experimental design structure view of rehabilitation robot device.

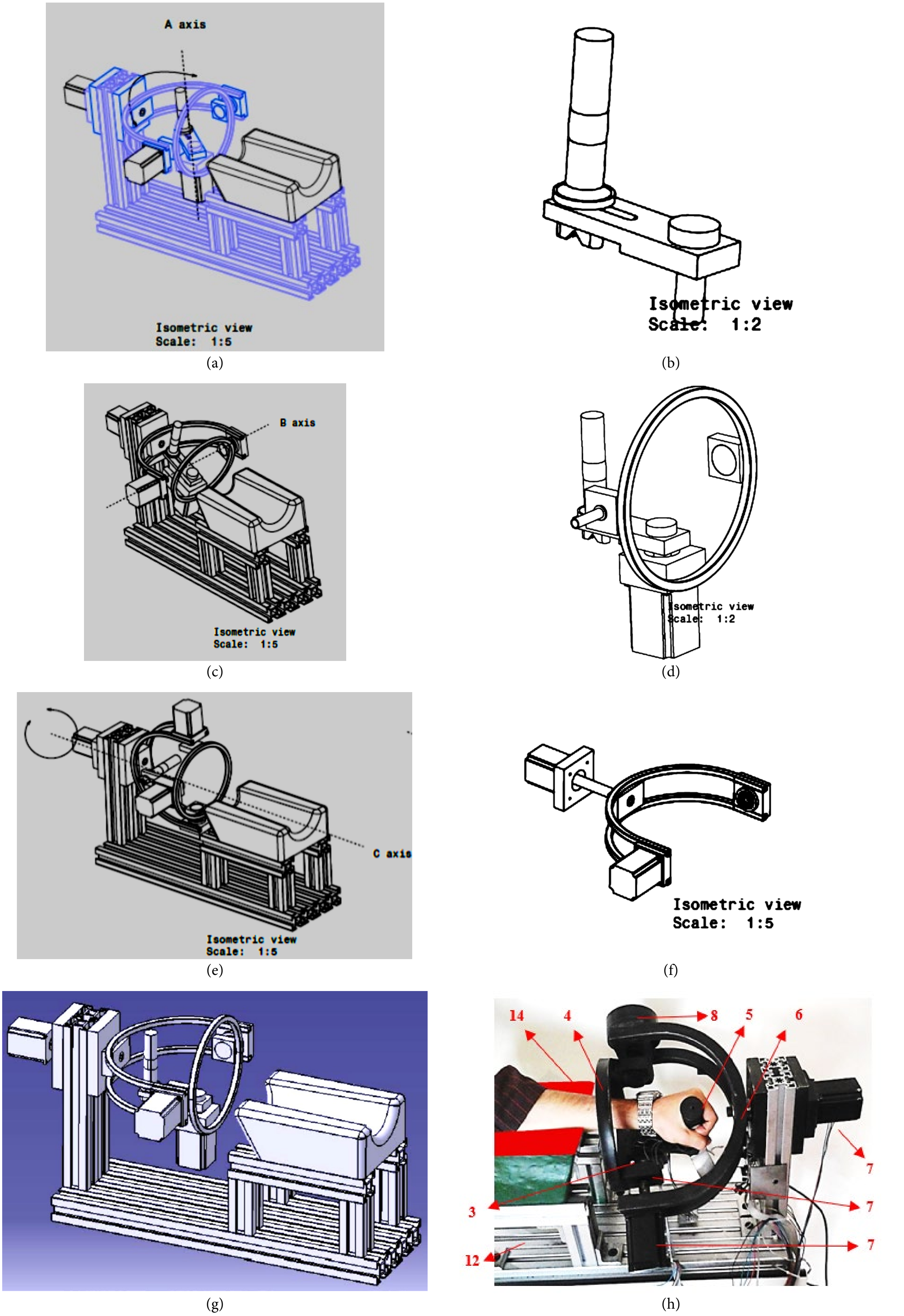

Figure 16. Mechanical structure of the rehabilitation robot device: (a) complete assembly of the horizontal arm (linear axis A); (b) detail view of the horizontal arm; (c) complete assembly of the vertical arm (linear axis B); (d) detailed view of the vertical arm; (e) complete assembly of the rotational arm (rotational axis C); (f) detailed view of the rotational arm; (g) designed view; and (h) experimental/constructed views.

Table 9.
List of electrical and electronic components utilized in the construction of the wrist joint rehabilitation robot.

Component	Quantity (Unit)	Description
IC	1	IC MAX 232, utilized for serial communication
Port	1	USB serial I/O port, enabling data transmission and reception
Sensor	2	IR optical sensor for detecting wrist position and movement
Sensor	4	FSR sensor, employed for pressure detection in the system
Sensor	4	Micro switch sensor for detecting specific positions or states of the robot components
Actuator	3	Stepper motors, for precise control of joint movement, including drivers and actuators
Driver	3	Drivers for stepper motors, responsible for controlling motor operation
Regulator	1	Voltage regulator 7805, ensuring stable voltage output for electronic components
IC	1	IC MAX 232, utilized for serial communication
Port	1	USB serial I/O port, enabling data transmission and reception
Sensor	2	IR optical sensor for detecting wrist position and movement
Sensor	4	FSR sensor, employed for pressure detection in the system

Table 10.
List of control system components used in the construction of the wrist joint rehabilitation robot.

Component	Quantity (Unit)	Description
Microcontroller	1	ATMEGA 32, used as the core controller for managing robot operations
Port/interface	1	USB-SERIAL converter, enabling communication between external devices
Connections	–	As required, for interfacing various components of the control system
Compiler	–	BASCOM-AVR Compiler, used for programming the ATMEGA 32 microcontroller
LabVIEW	–	LabVIEW, used for visual programming and control of system operations
Microcontroller	1	ATMEGA 32, used as the core controller for managing robot operations

III. Results and Discussions

In simulation, Figure 17 illustrates wrist motion patterns generated by the rehabilitation robot across three modes. In mode A (passive), the robot moves the wrist without patient effort, producing high-amplitude, smooth sinusoidal curves, particularly in flexion/extension and pronation/supination. In mode B (assistive), the robot supports partial movement, reducing amplitudes slightly to encourage patient engagement. mode C (muscle strengthening and resistive) introduces resistance, requiring full patient effort, with lower amplitudes.

All modes follow periodic trajectories over 0 s to 6.5 s, reflecting progressive rehabilitation from passive mobility to active strengthening. Figure 18(a) compares torque, force, acceleration, and velocity of the H.W.R.R in the three modes vs. a reference. Torque and force steadily increase from mode A to mode C, indicating greater muscular involvement. Acceleration peaks in mode C (1.80 rad/s^2), surpassing the reference, indicating active engagement. Velocity remains stable around 0.50 rad/s to 0.55 rad/s, ensuring controlled motion.

Overall, the robot progressively increases effort demands while maintaining consistent movement, supporting rehabilitation. Figure 18(b) shows the progressive performance increase of the H.W.R.R from mode A to mode C. Torque rises from 0.60 N·m to 1.00 N·m, and force increases from 6.50 N to 11.00 N, approaching reference values. Angular acceleration peaks at 1.80 rad/s^2 in mode C, exceeding the reference, while angular velocity stays between 0.50 rad/s to 0.55 rad/s, indicating controlled but intensifying motion. Figure 19 combines the performance of each mode across the four parameters in a single graph. It highlights the progressive enhancement in performance from mode A (mode 1) to mode C (mode 3) with mode C showing the highest values for all parameters.

The reference line serves as a baseline, and while mode C nearly matches or surpasses the reference in angular parameters, it remains below in torque and force, suggesting an optimized balance between performance and mechanical stress.

Finally, Figure 20 tracks the variation of each parameter across modes. Torque and force steadily rise from mode A to mode C, with the gap to the reference remaining visible. In contrast, angular acceleration and velocity show closer proximity to the reference, reflecting good dynamic response characteristics

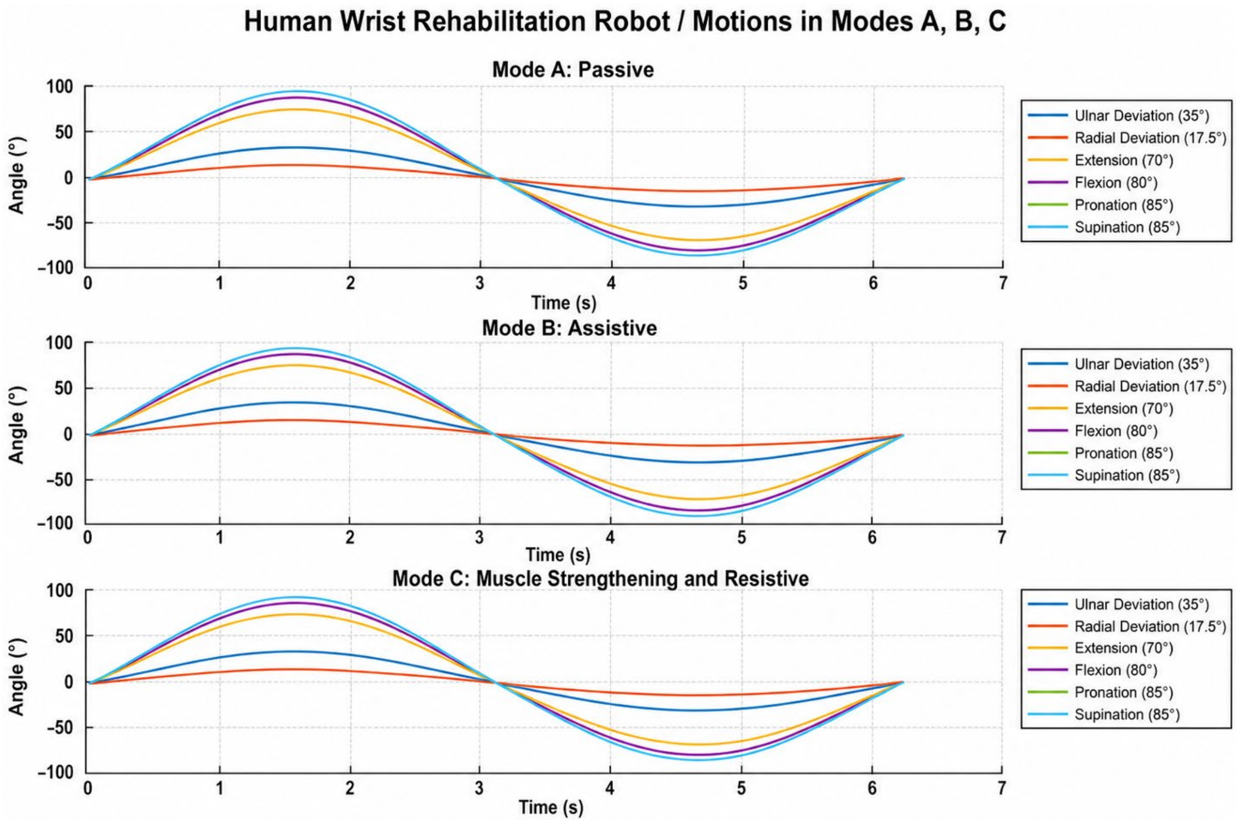

Figure 17. Simulation signals of H.W.R.R motions in modes.

(Table 11). Simulation results (Figure 17 and Figure 18) show torque, velocity, and angular position tracking. The microcontroller-based control integrates FSR sensors, stepper motors, and LabVIEW interface to achieve coordinated motion with precise feedback, ensuring accurate force application during rehabilitation. The reliability of the wrist rehabilitation robots in this research was assessed using the people's t-test for both male and female participants. Table 12 presents the t-test results for males and Table 13 for females, including parameters such as SE, ICC, CV, p-value, and SD. The results confirm high repeatability and consistency of the robot's performance across both groups.

Table 12 and Table 13 show high reliability and consistency of the wrist rehabilitation robot for both male and female participants. The very low SDs in wrist angle indicate precise and stable joint motion, supporting effective stiffness reduction through controlled and repeatable movements. Low CVs and highly significant p-values ($p < 0.001$) confirm uniform and reliable assisted motion across trials. Additionally, the high ICC values for torque demonstrate consistent load application, which is essential for safe and progressive muscle strengthening. Overall, these results justify the rehabilitation benefits of the robot by enabling stiffness reduction, reliable assisted movement, and controlled muscle strengthening in wrist rehabilitation.

In the experimental data, Figure 21 shows MATLAB plots comparing SD, SE, CV, and ICC for angles, accelerations, and torque. Angles have low SD and SE, indicating precision, while accelerations and torque show higher SD and SE, suggesting variability. Torque and accelerations have high ICC, indicating reliability, while angles, particularly Angle1, have low

Table 11.
Comparing this work robot with recent studies.

Study	Control Type	DOF	Max Torque (N·m)	Max Velocity (rad/s)	Notes
This work	AFC-PID	3	1.00	0.55	Phase-based rehab modes, adaptive torque
Smith *et al.*, 2022	PID	2	0.75	0.50	Passive/assistive only
Lee *et al.*, 2021	Fuzzy-PID	3	0.90	0.52	No resistive mode
Chen *et al.*, 2023	Sliding mode	3	0.95	0.53	Limited clinical testing

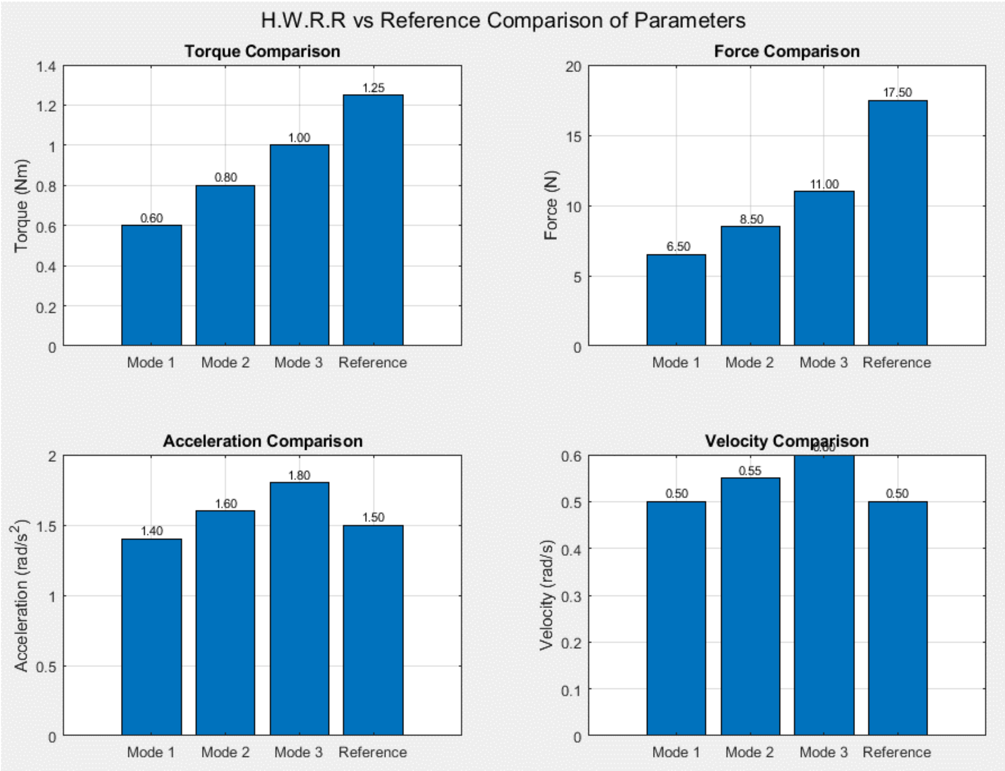

(a)

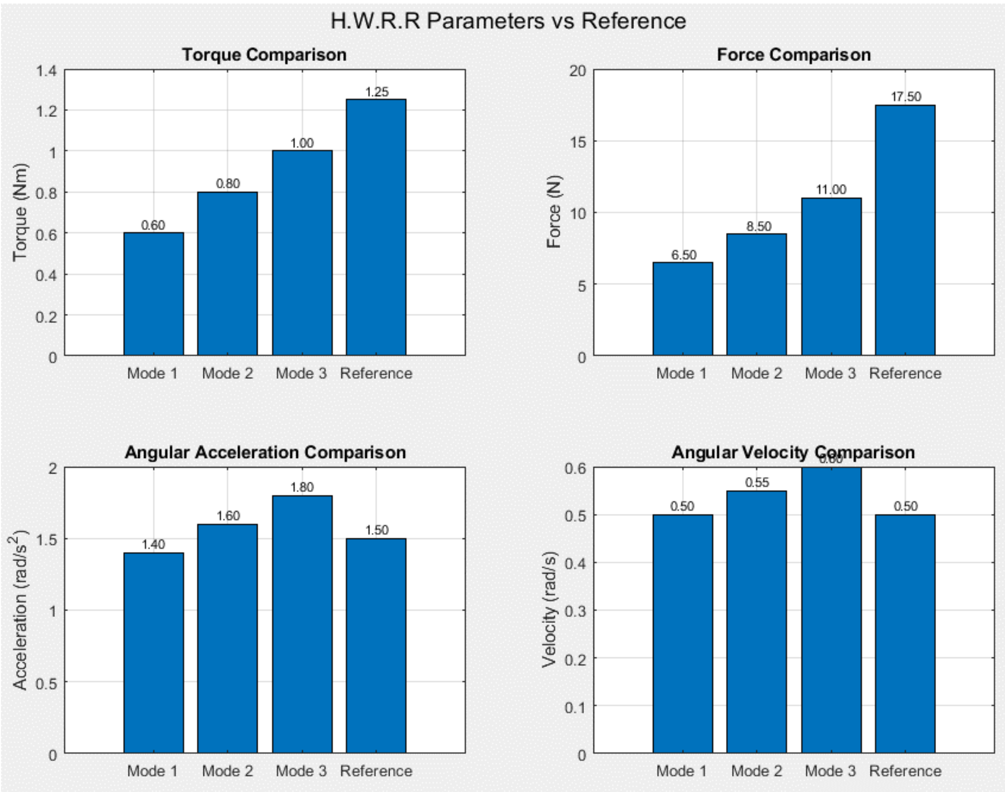

(b)

Figure 18. Simulation parameters signal comparison vs. reference of H.W.R.R: (a) H.W.R.R vs. reference comparison of parameters; (b) H.W.R.R parameters vs. reference.

ICC, suggesting inconsistency. Figure 22(a) shows greater SD variability in the reference group for angles (e.g., Angle2: 0.00444) compared to male (0.0013) and female (0.0016).

Acceleration variability is higher (e.g., Accel2: 1.959), and torque shows slight variation, higher in reference (0.40523) and female (0.42). Figure 22(b) shows the lowest SE for male in angles and accelerations, but high SE for torque (0.70), indicating inconsistency. Figure 23(a) reveals the highest CV for angles in the reference group (e.g., Angle2: 0.2022), suggesting poor stability, while torque shows consistent CV across groups (CV < 0.021). Figure 23(b) shows ICC values above 0.90, indicating excellent reliability.

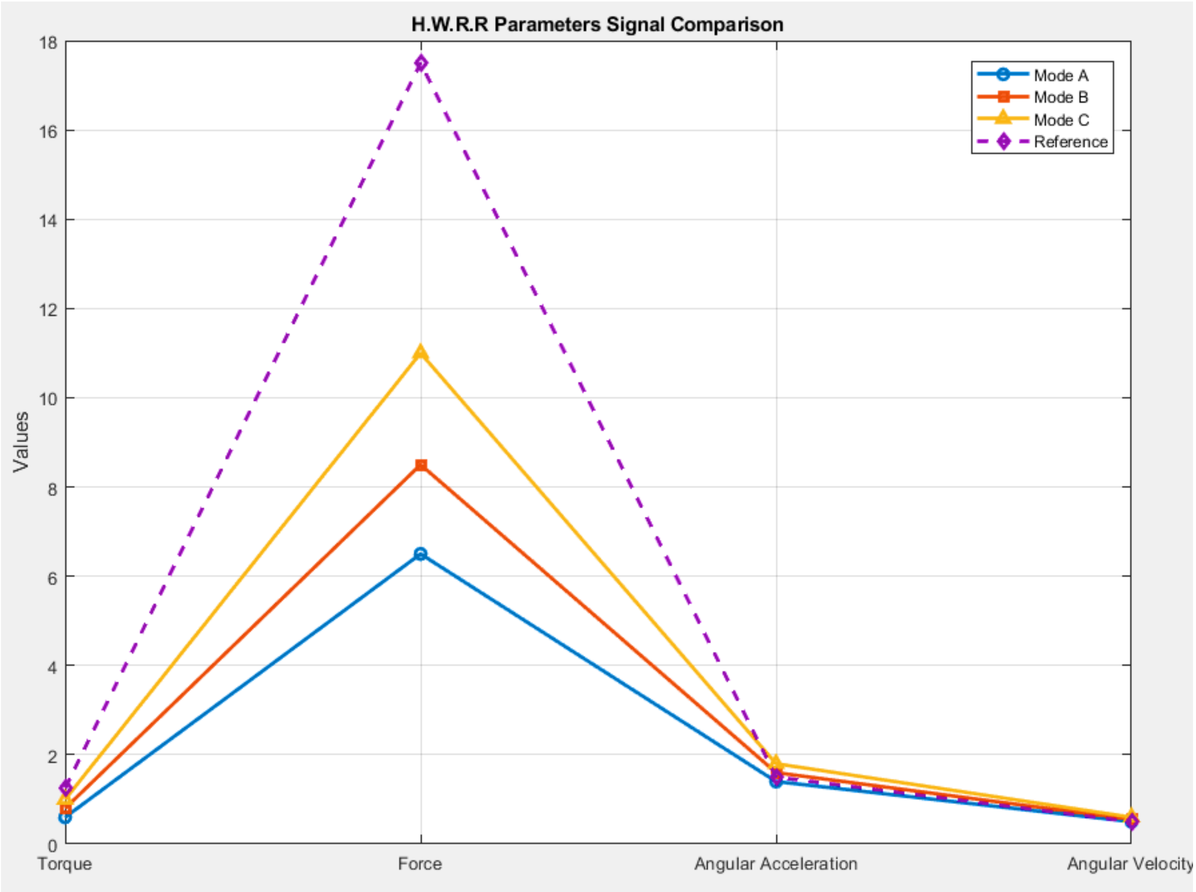

Figure 19. H.W.R.R parameters signal comparison.

Table 12.
Results of the male's t-test of wrist rehabilitation robots.

Gender	Parameter	SD	*p*-value	CV	ICC	SE
Male	Angle (rad)	0.0011	0.000	0.11	0.980	0.00025
	Angle (rad)	0.0013	0.000	0.10	0.985	0.00028
	Angle (rad)	0.0015	0.000	0.09	0.990	0.00030
	Acceleration (m/s^2)	1.48	0.000	0.11	0.991	0.30
	Acceleration (m/s^2)	1.60	0.000	0.12	0.993	0.35
	Acceleration (m/s^2)	1.62	0.000	0.10	0.995	0.36
	Torque (N·m)	0.39	0.000	0.018	0.998	0.70

Table 13.
Results of the female's t-test of wrist rehabilitation robots.

Gender	Parameter	SD	*p*-value	CV	ICC	SE
Female	Angle (rad)	0.0013	0.000	0.12	0.975	0.00030
	Angle (rad)	0.0016	0.000	0.11	0.980	0.00033
	Angle (rad)	0.0018	0.000	0.10	0.982	0.00035
	Acceleration (m/s^2)	1.60	0.000	0.12	0.985	0.33
	Acceleration (m/s^2)	1.72	0.000	0.13	0.988	0.38
	Acceleration (m/s^2)	1.75	0.000	0.11	0.989	0.39
	Torque (N·m)	0.42	0.000	0.021	0.995	0.078

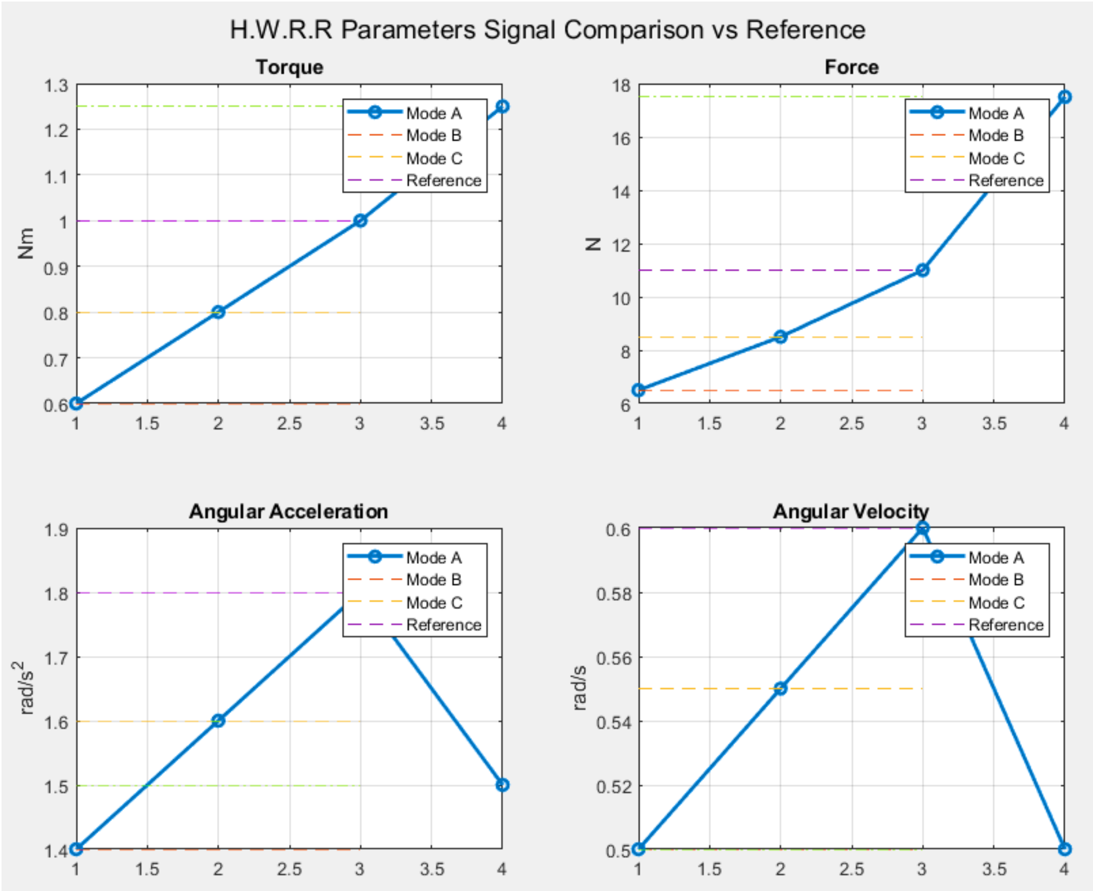

Figure 20. H.W.R.R parameters signal comparison vs. reference.

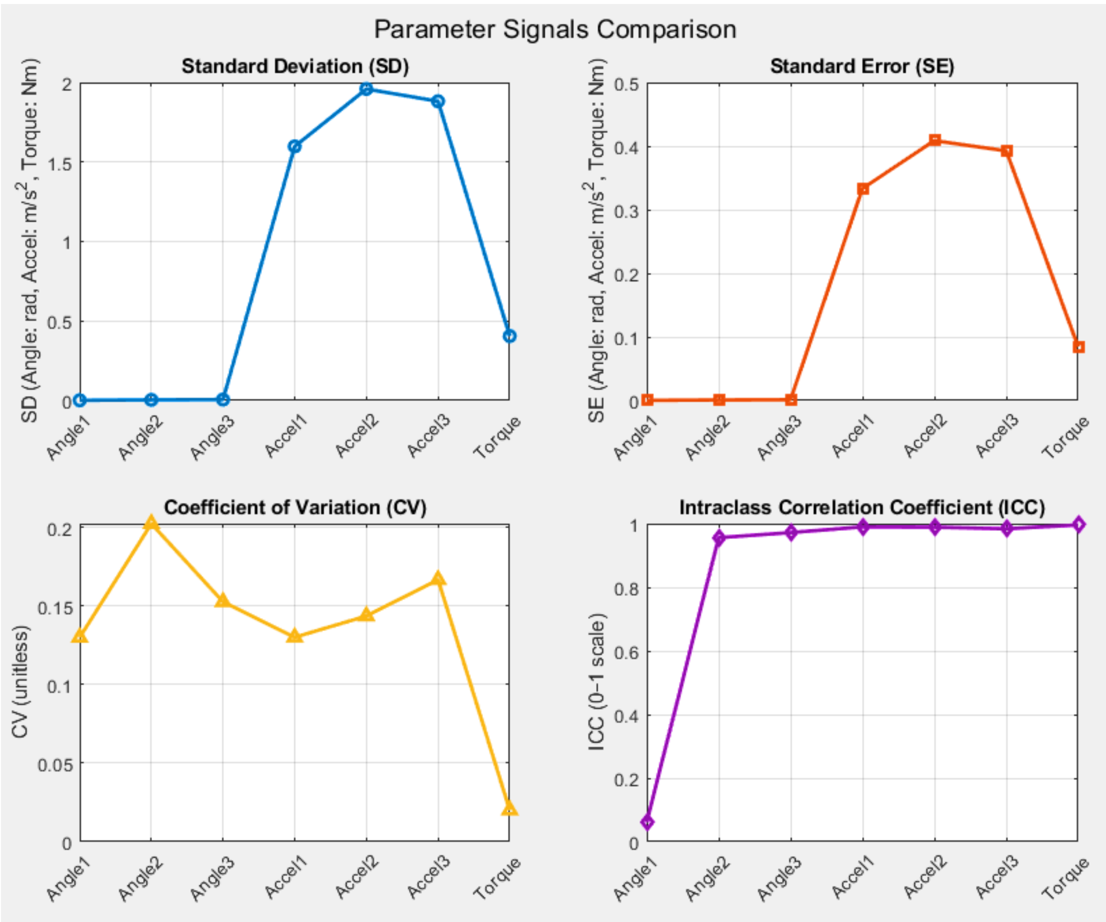

Figure 21. Parameter signals comparison in line graph.

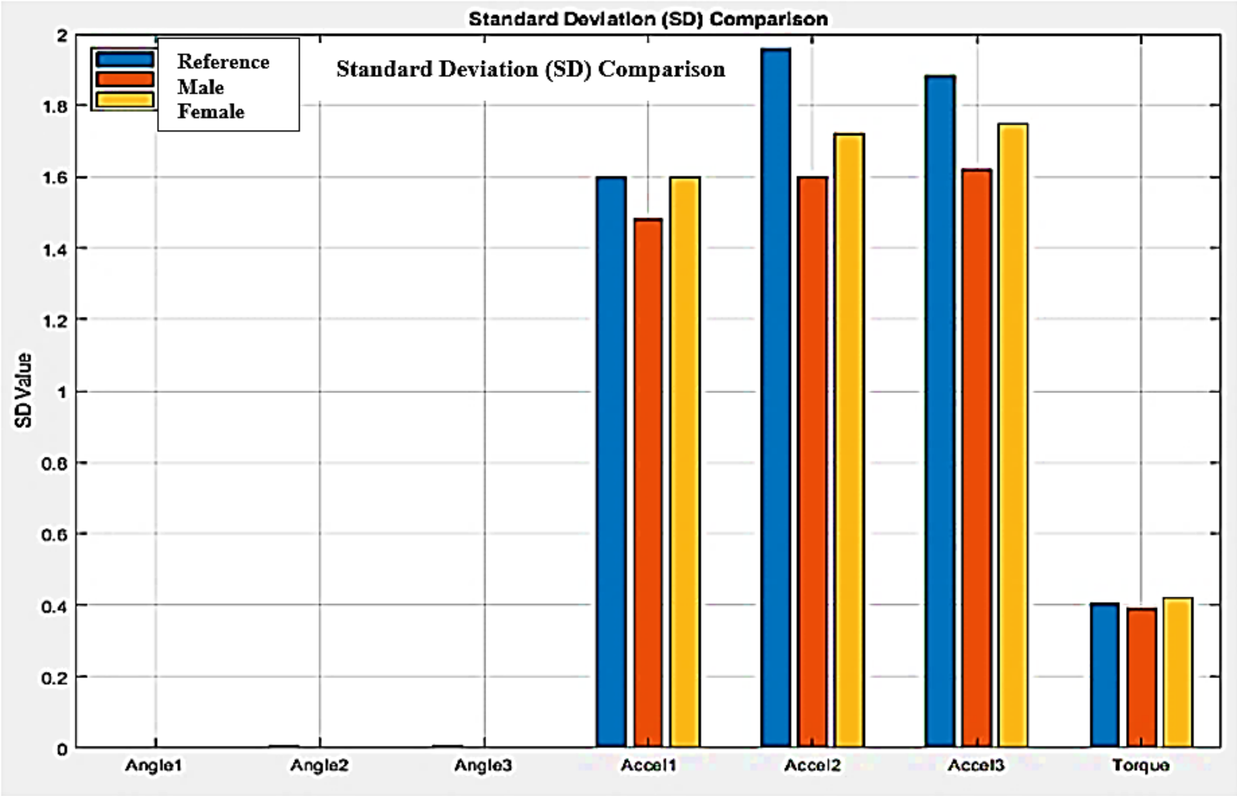

(a)

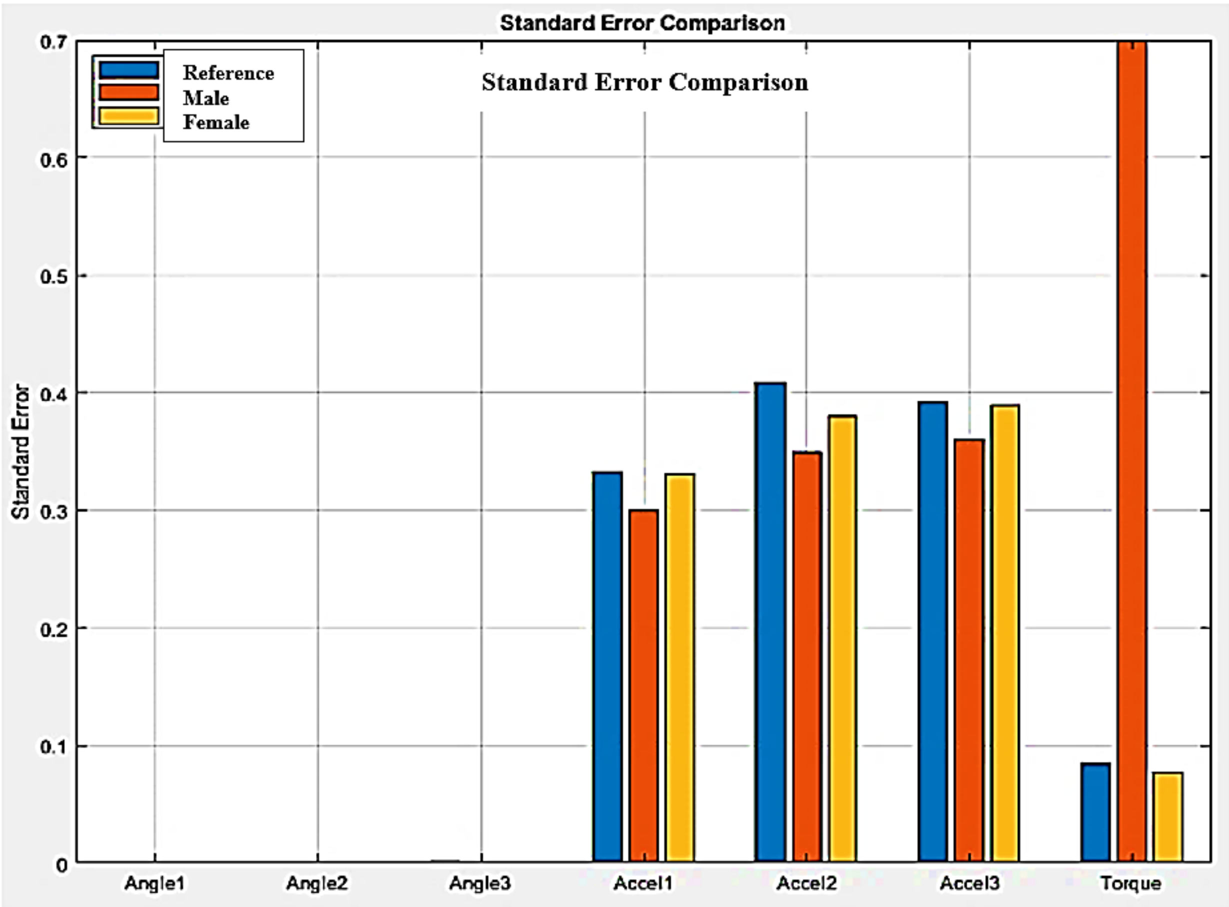

(b)

Figure 22. Experimental parameters signal comparison vs. reference of H.W.R.R: (a) SD comparison in bar chart; (b) SE comparison in bar chart.

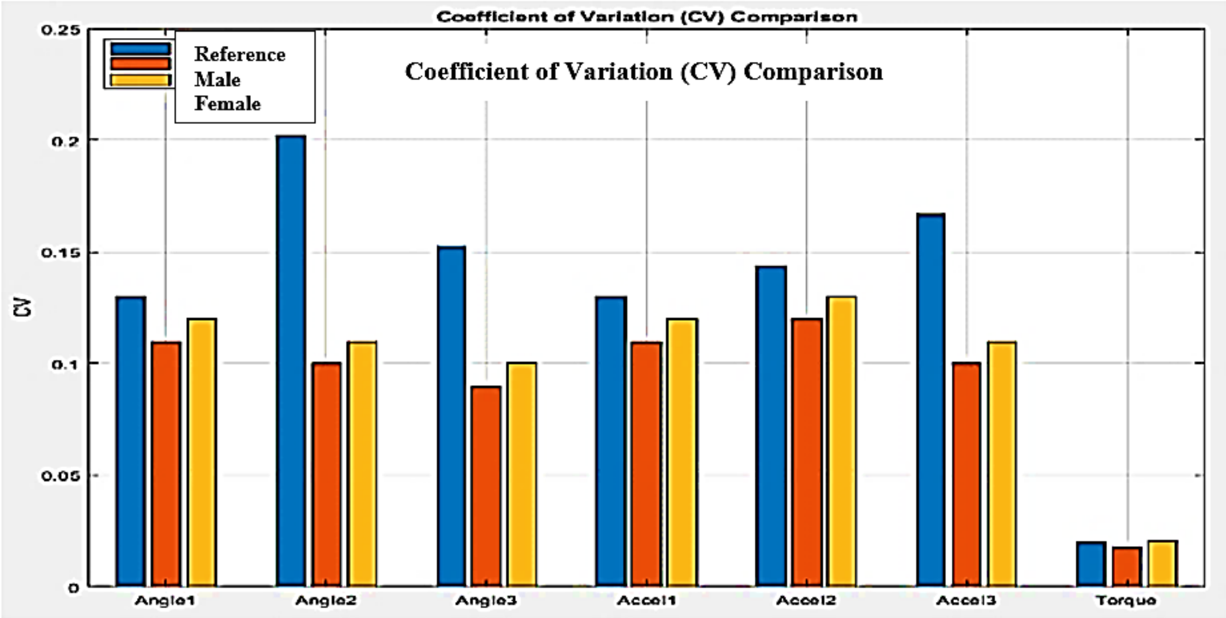

(a)

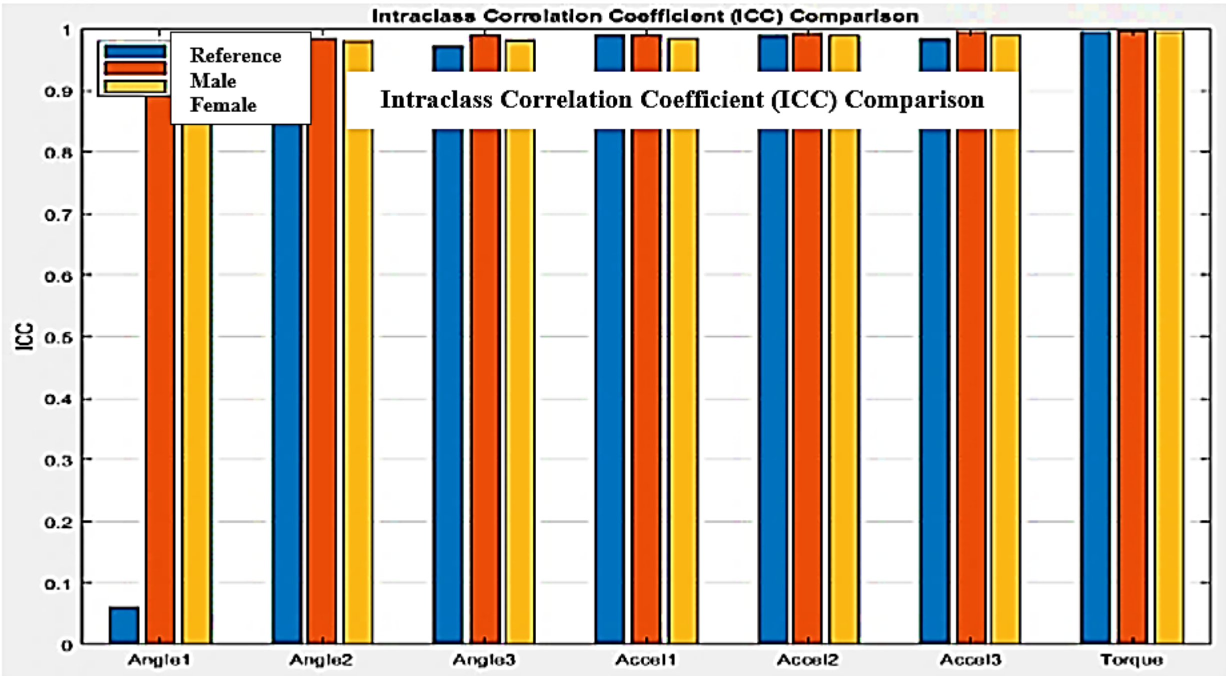

(b)

Figure 23. (a) CV comparison in bar chart; (b) ICC comparison in bar chart.

Male and female groups show high reliability (ICC > 0.98) for angles, while the reference group has a low ICC for Angle1 (0.0616), suggesting instability. Figure 24(a) shows SD values, with the reference group having the highest variability (0.00144 to 1.959), and male showing lower variation. Torque has the highest SD, indicating variability, while angular measurements are consistent. Figure 24(b) shows the highest SE in the reference group (0.000302 to 1.959), indicating higher sampling error, with lower SE in male and female. Figure 25(a) shows the reference group has the highest CV (0.0201 to 0.2022), indicating greater variability, while Male and Female show more consistent angular measurements. Finally, Figure 25(b)) reveals lower ICC values for the reference group (0.0616 to 0.996), indicating poor consistency, while Male and Female have high ICC (ICC > 0.98), indicating reliability, with torque showing the highest ICC across all groups.

Mode C exceeding the reference in angular acceleration reflects active engagement by the patient, crucial for muscle strengthening. Higher SD in angles

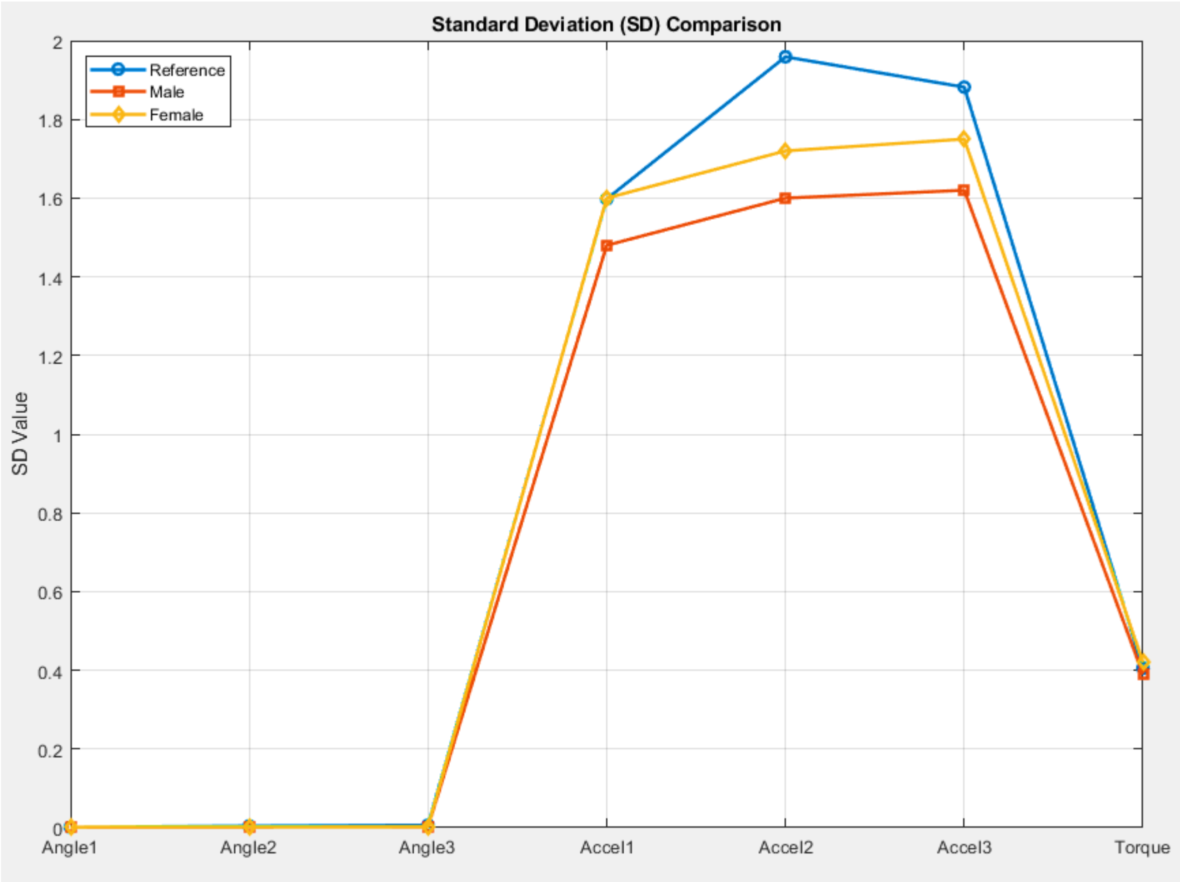

(a)

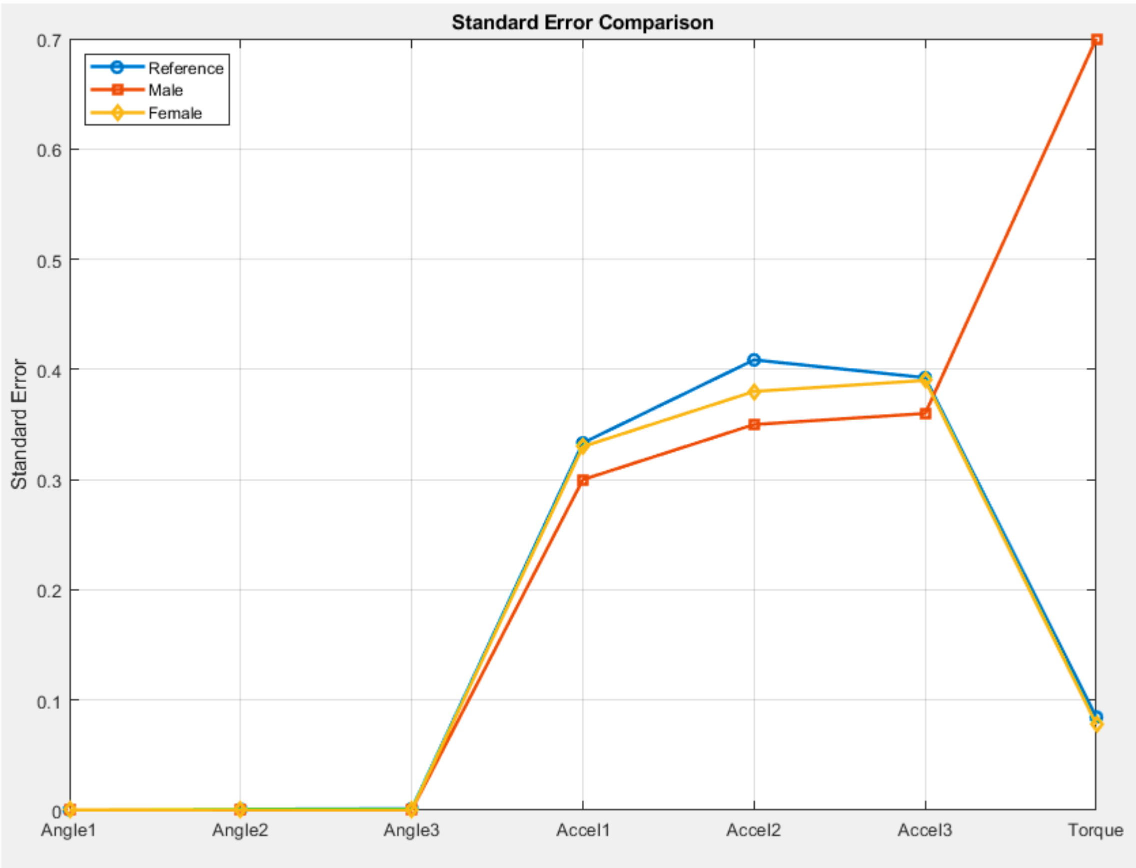

(b)

Figure 24. (a) SD comparison in line graph and (b) SE comparison in line graph.

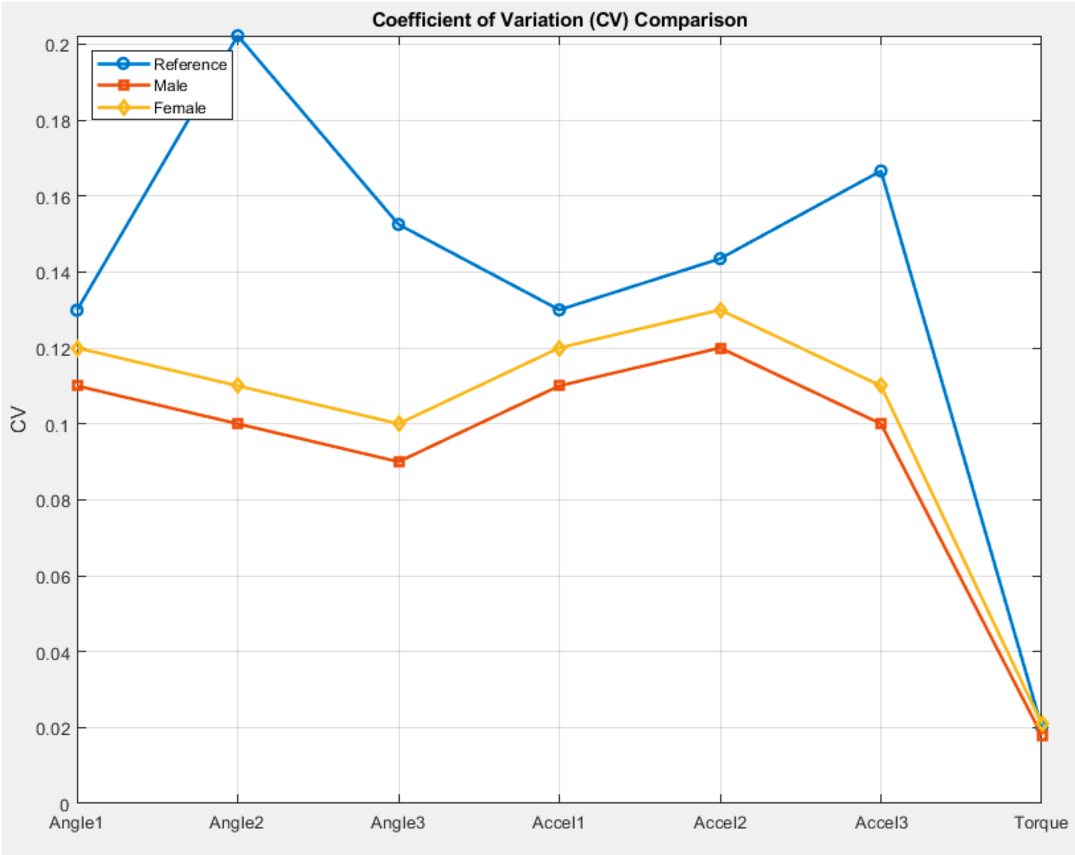

(a)

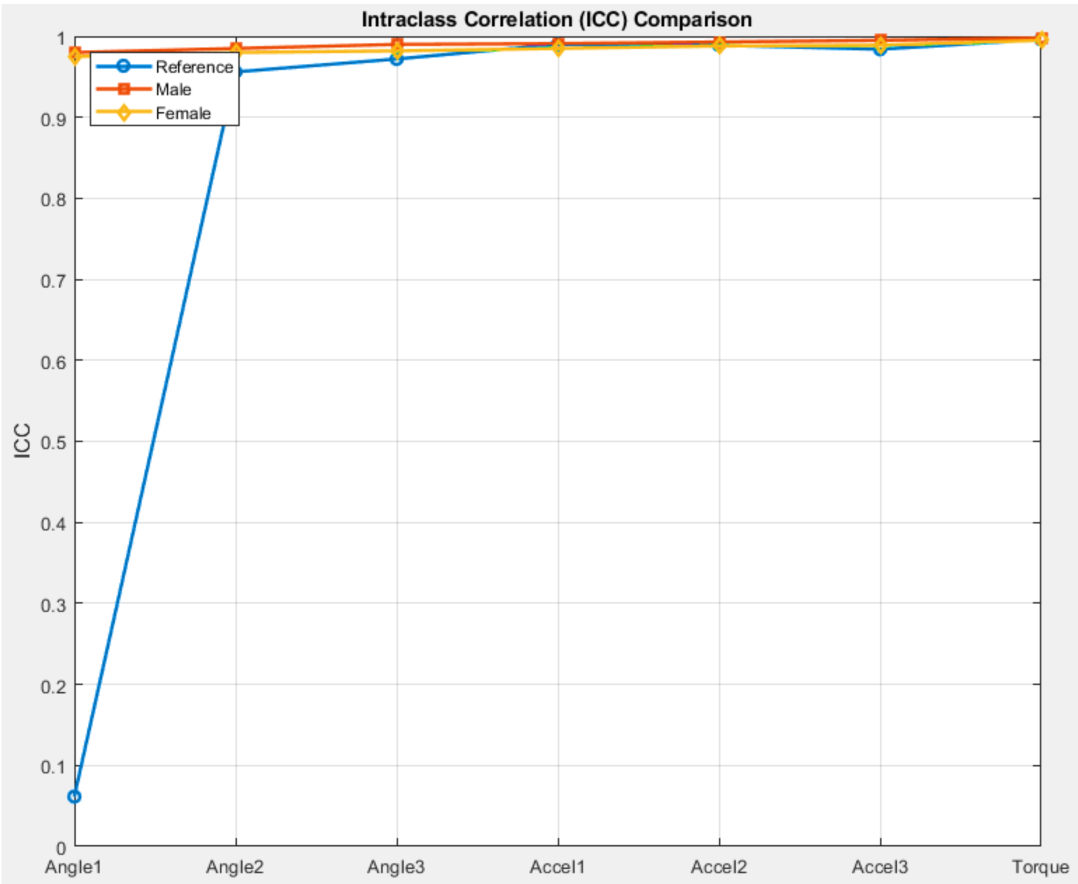

(b)

Figure 25. (a) CV comparison in line graph; (b) ICC comparison in line graph.

indicates variability among users, highlighting the need for individualized therapy adjustments. The steady increase in torque and force aligns with rehabilitation goals of progressive resistance training, ensuring safe yet challenging motion for recovery.

IV. Conclusion

In this study, a wrist rehabilitation robot was designed and developed with the ability to perform 18 distinct movements across three modes: passive, assistive, and resistive. The results demonstrated that the robot effectively covers the full range of wrist motion, assists patients with limited muscle strength in assistive mode, and strengthens muscles in resistive mode. Key features include high motion accuracy, ergonomic design, adaptive control, and the ability to monitor and record therapy progress. With successful clinical performance and commercialization potential, the robot represents an innovative and effective solution for wrist rehabilitation. This study highlights the potential of robotic systems in wrist rehabilitation, providing an efficient, accessible, and precise alternative to traditional methods. The 3-DOF robotic system, operating in passive, assisted, and muscle strengthening modes, effectively addresses muscle relaxation, movement completion, and strengthening, as demonstrated in the experimental results. Advanced control algorithms and sensors allow the robot to adapt to individual patient needs, improving therapeutic outcomes. Table 1 and Table 2 emphasize the structured, phase-based approach, with Table 2 standardizing motion ranges across subjects, independent of gender, ensuring consistency and safety. The system's progression through modes reduces the risk of overextension or injury. Gender-independent targets further enhance clinical and robotic rehabilitation applications. Table 3's gender-specific data shows that males generally exhibit higher torque and force, while females may perform better in endurance and control, providing valuable insights for personalized designs in robotics and prosthetics. High repeatability, validated by t-test results (Table 12 and Table 13), and strong consistency, indicated by low SEs and high ICC, confirm the system's reliable performance. Overall, this study demonstrates the advantages of a phase-based, gender-sensitive robotic system in wrist rehabilitation, combining standardized motion protocols, personalized performance data, and high reliability to support clinical use and patient recovery. Limitations of the current system include the relatively large size and fixed workstation of the robot, limiting portability; absence of long-term clinical trials to validate sustained efficacy; and assumptions in mode C that the patient can exert sufficient force to overcome resistive torques without overextension. The primary novel contribution of this work is the integration of AFC with PID in a 3-DOF wrist robot, enabling adaptive torque compensation, high repeatability, and phase-based rehabilitation tailored to patient-specific capabilities. Future work includes clinical trials to validate therapeutic outcomes, miniaturization of the device for portable applications, and integration of biofeedback systems to enhance patient engagement and adaptive control.

Acknowledgements

The authors would like to express sincere gratitude to the Faculty of Engineering, Science and Technology, and the affiliated institution for providing the academic environment, facilities, and support necessary for conducting this research. The author also appreciates the valuable contributions of researchers whose published works formed the foundation of this research and review study.

Declarations

Author contribution

A. Moloody, M. Mahjoob, A. As’arry, and M.Z. Md Zain designed, fabricated, implemented, and evaluated the proposed system and conducted all experimental work and data analysis presented in this study. The author confirms that all results presented are original and that the manuscript has not been published elsewhere. All data generated and analyzed during this study are included in the manuscript. All authors read and approved the final paper.

Funding statement

This research did not receive any specific grant from funding agencies in the public, commercial, or not-for-profit sectors.

Competing interest

The authors declare that they have no known competing financial interests or personal relationships that could have appeared to influence the work reported in this paper.

Additional information

Reprints and permission: information is available at https://mev.brin.go.id/.

Publisher’s Note: National Research and Innovation Agency (BRIN) remains neutral with regard to jurisdictional claims in published maps and institutional affiliations.

References

[1] G. F. Garcia, R. S. Gonçalves, and G. Carbone, "A review of wrist rehabilitation robots and highlights needed for new devices," *Machines*, 12(5): 315, 2024.

[2] S. Li, Z. Wang, Z. Pang, M. Gao, and Z. Duan, "Design and analysis of a hemispherical parallel mechanism for forearm–wrist rehabilitation," *Appl. Bionics and Biomech.*, 2023(1), 2023.

[3] T. Goyal, S. Hussain, E. Martinez-Marroquin, N. A. T. Brown, and P. K. Jamwal, "Stiffness-observer-based adaptive control of an intrinsically compliant parallel wrist rehabilitation robot," *IEEE Trans. Hum. Mach. Syst.*, 53(1): 65–74, 2022.

[4] V. E. Abarca and D. A. Elias, "A review of parallel robots: Rehabilitation, assistance, and humanoid applications for neck, shoulder, wrist, hip, and ankle joints," *Robotics*, 12(5): 131, 2023.

[5] G. Alonso-Linaje, A. Cisnal, J. C. Fraile, and J. P. Turiel, "Design and analysis of the M3Rob: A robotic platform for wrist and hand rehabilitation," *IEEE Access*, 12: 30472–30481, 2024.

[6] L. Zhang, Z. Yu, P. Su, J. Li, and R. Ge, "Design of a parallel wrist rehabilitation robot and analysis of physiological effect on training," *IEEE/ASME Trans. Mechatron.*, 29(5): 3401–3414, 2024.

[7] H. Lee, W. Kim, J. Han, and C. Han, "The technical trend of the exoskeleton robot system for human power assistance," *Int. J. Precision Eng. Manuf.*, 13(8): 1491–1497, 2012.

[8] Y. Zhao *et al.*, "Adaptive cooperative control strategy for a wrist exoskeleton using model-based joint impedance estimation," *IEEE/ASME Trans. Mechatron.*, 28(2): 748–757, 2023.

[9] B. Saeedi, M. M. Moghaddam, and M. Sadedel, "Conceptual design and characteristics of a new wrist rehabilitation exoskeleton based on systematic approach," in *11th RSI International Conference on Robotics and Mechatronics (ICRoM)*, pp. 457–463, 2023.

[10] B. Saeedi, M. Mohammadi Moghaddam, and M. Sadedel, "Inverse kinematics analysis of a wrist rehabilitation robot using artificial neural network and adaptive neuro-fuzzy inference system," *Mech. Based Des. Struct. Mach.*, 52(12): 10439–10487, 2024.

[11] A. S. N. Husainy, S. Mangave, and N. Patil, "A review on robotics and automation in the 21st century: shaping the future of manufacturing, healthcare, and service sectors," *Asian Review of Mechanical Engineering*, 12(2): 41–45, 2023.

[12] J. A. DeLisa, *Physical medicine and rehabilitation: principles and practice*, 4th ed., 2100 pages, 2004.

[13] J. H. Carr and R. B. Shepherd, *Neurological rehabilitation: Optimizing motor performance*, 364 pages, 2003.

[14] T. Nef, M. Mihelj, and R. Riener, "ARMin: A robot for patient-cooperative arm therapy," *Med Biol Eng Comput*, 2007, 45: 887–900, 2007.

[15] B. Saeedi, M. Sadedel, and M. Moghaddam, "Innovative integration of meta-heuristic algorithms with adaptive TSK fuzzy systems for inverse kinematics in a new wrist and forearm rehabilitation exoskeleton," *Iran. J. Sci. Technol. - Trans. Mech. Eng.*, 49(2): 927–962, 2025.

[16] C. Greco, T. H. Weerakkody, V. Cichella, L. Pagnotta, and C. Lamuta, "Lightweight bioinspired exoskeleton for wrist rehabilitation powered by twisted and coiled artificial muscles," *Robotics*, vol. 12, no. 1, 2023.

[17] P. Gu, "Modular design and control system optimisation of an upper limb rehabilitation robot," *Highlights in Science, Engineering and Technology*, vol. 134, pp. 163–170, 2025.

[18] P. Sale, V. Lombardi, and M. Franceschini, "Hand robotics rehabilitation: Feasibility and preliminary results of a robotic treatment in patients with hemiparesis," *Stroke Research and Treatment*, vol. 2012, Art. no. 820931, 2012.

[19] A. Schweikard and F. Ernst, *Medical Robotics*. Lübeck, Germany: Institute for Robotics and Cognitive Systems, University of Lübeck.

[20] Q. Liu *et al.*, "Path planning and impedance control of a soft modular exoskeleton for coordinated upper limb rehabilitation," *Frontiers in Neurorobotics*, vol. 15, Art. no. 745531, 2021.

[21] N. Hamilton, W. Weimar, and K. Luttgens, *Kinesiology: Scientific Basis of Human Motion*, 11th ed. New York, NY, USA: McGraw-Hill, 2007.

[22] D. A. Winter, *Biomechanics and Motor Control of Human Movements*, 2nd ed. Waterloo, Canada: University of Waterloo Press, 1992.

[23] A. Basteris *et al.*, "Training modalities in robot-mediated upper limb rehabilitation in stroke: A framework for classification based on a systematic review," *Journal of NeuroEngineering and Rehabilitation*, vol. 11, Art. no. 111, 2014.

[24] O. Mehrez *et al.*, "Development of an exoskeleton for wrist-joint rehabilitation: Modeling, identification, and control," *Multibody System Dynamics*, 2025.

[25] P. Tucan *et al.*, "Design and experimental setup of a robotic medical instrument for brachytherapy in non-resectable liver tumors," *Cancers*, vol. 14, Art. no. 5841, 2022.

[26] C. Vaida *et al.*, "Innovative development of a spherical parallel robot for upper limb rehabilitation," *International Journal of Mechanical and Robotics Systems*, vol. 4, p. 256, 2018.

[27] M. K. Burns, D. Pei, and R. Vinjamuri, "Myoelectric control of a soft hand exoskeleton using kinematic synergies," *IEEE Transactions on Biomedical Circuits and Systems*, vol. 13, pp. 1351–1361, 2019.

[28] A. Chowdhury, S. S. Nishad, Y. K. Meena, A. Dutta, and G. Prasad, "Hand-exoskeleton assisted progressive neurorehabilitation using impedance adaptation based challenge level adjustment method," *IEEE Transactions on Haptics*, vol. 12, pp. 128–140, 2019.

[29] L. Gerez, G. Gao, A. Dwivedi, and M. Liarokapis, "A hybrid, wearable exoskeleton glove equipped with variable stiffness joints, abduction capabilities, and a telescopic thumb," *IEEE Access*, vol. 8, pp. 173345–173358, 2020.

[30] J. Iqbal, H. Khan, N. G. Tsagarakis, and D. G. Caldwell, "A novel exoskeleton robotic system for hand rehabilitation—conceptualization to prototyping," *BioCybernetics and Biomedical Engineering*, vol. 34, pp. 79–89, 2014.

[31] H. Ren and H. Zhang, "Control strategy based on improved fuzzy algorithm for energy control of wrist rehabilitation robot," *Alexandria Engineering Journal*, vol. 77, pp. 634–644, 2023.

[32] M. Abbas, A. Azizan, S. H. Tang, K. Raja, and Z. Ali, "PID controller parameter tuning based on a modified differential evolutionary optimization algorithm for the intelligent active vibration control of a combined single-link robotics flexible manipulator," *Journal of Advanced Research in Applied Sciences and Engineering Technology*, vol. 52, no. 1, pp. 233–258, 2024.

[33] M. Abbas, A. Azizan, S. H. Tang, K. Raja, and B. Irfan, "Analysis, modelling, and simulation for the intelligent active vibration control of a combined plant using a new gyroscopic combined actuator model," *Journal of Advanced Research in Applied Sciences and Engineering Technology*, vol. 63, no. 1, pp. 102–129, 2024.

[34] Q. Wang *et al.*, "Modular design and implementation of upper limb exoskeleton rehabilitation robot: Structure, force sensor and control," in *Proc. Chinese Control Conf. (CCC)*, 2023, pp. 4568–4573.

[35] B. H. Dobkin, "Rehabilitation after stroke," *New England Journal of Medicine*, vol. 352, pp. 1677–1684, 2005.

[36] M. Abbas, A. Azizan, S. H. Tang, K. Raja, and Y. Zuhri, "A comprehensive review based on analysis modeling, mechanical vibration control strategies, and optimization methods of robotics flexible manipulator structures," *Pertanika Journal of Science and Technology*, vol. 33, no. 1, 2025.

[37] J. Pan *et al.*, "NESM-γ: An upper-limb exoskeleton with compliant actuators for clinical deployment," *IEEE Robotics and Automation Letters*, vol. 7, no. 3, pp. 7708–7715, 2022.

[38] M. Abbas, A. Azizan, S. H. Tang, and K. Raja, "An experimental study on the mechatronics design and implementation of an intelligent active vibration control system for a CSLRFM," *Journal of Advanced Research in Applied Mechanics*, vol. 134, no. 1, 2025.